April 2014

OXYGEN GENERATION THROUGH ELECTRICALLY STIMULATED O2 REDUCTION ACROSS ION EXCHANGE MEMBRANES

Daniel Rodgers Jones
Worcester Polytechnic Institute

Devin A. Churchman
Worcester Polytechnic Institute

Raj D. Patel
Worcester Polytechnic Institute

OXYGEN GENERATION THROUGH ELECTRICALLY STIMULATED O_2 REDUCTION ACROSS ION EXCHANGE MEMBRANES

A Major Qualifying Project Report

Submitted to the Faculty of

WORCESTER POLYTECHNIC INSTITUTE

In partial fulfillment of the requirements

for the Degree of Bachelor of Science

by

_____

Devin Churchman, CM

_____

Daniel Jones, CH

_____

Raj Patel, CM

April 30, 2014

Approved:

_____

Professor Ravindra Datta, Major Advisor

_____

Professor Stephen J. Kmiotek, Co-Advisor

_____

Professor Drew Broduer, Co-Advisor

Table of Contents

List of Tables 4

List of Figures 5

Abstract 6

1. Introduction 7

2. Literature Review 10

2.1 Social Implications 10

2.1.1 Diseases and Conditions 10

2.1.2 Current Solutions 11

2.2 Chemistry 13

2.2.1 Four Electron Oxygen Reduction Reactions 13

2.2.2 Two Electron Oxygen Reduction Reactions 14

2.3 Proton Exchange Membrane (PEM) 18

2.3.1 Introduction to PEMs 18

2.3.2 Mechanism 19

2.3.3 Hydrogen Oxygen Fuel Cell 23

2.3.4 Oxygen generation case studies 25

2.4 Anion-Exchange Membrane (AEM) 33

2.4.1 Development 33

2.4.2 Mechanism 34

2.4.3 Benefits and Challenges 36

2.4.4 Oxygen Generation Case Studies 37

3. Methodology 38

3.1 Conceptual Design 38

3.2 Apparatus 40

3.3 Materials 42

3.4 Experimental 43

4. Results & Discussion 47

4.1 Liquid Electrolysis 47

4.2 Vapor Electrolysis 48

4.3 Two Electron Oxygen Reduction 52

4.4 Carbon Degradation 55

5. Conclusion and Recommendations 57
5.1 Conclusion 57
5.2 Recommendations 58
5.2.1 Use of Alternative Catalysts 58
5.2.2 Fabricating Membranes 60
5.2.3 Stacking 61
5.2.4 Anion Exchange Membranes 62
5.2.5 Mathematical Analysis 62
Works Cited 64
Appendix A: Results summary table 68
Appendix B: MEA P1 Results 76
IR Spectroscopy of MEA P1 77
Appendix C: U.S Patent 5,211,984 for Membrane Catalyst Loading in MEA Fabrication (Wilson, 1993) 78
Appendix D: Sample plot generated by COMSOL. 82

List of Tables

Table 2.1 A The Half Reaction and Overall Reaction for MA's O2 Concentrator (Ma & Yu, 1995) 12

Table 2.2 A The Four Electron Oxygen Reduction Reactions 13
Table 2.2 B Water Electrolysis 14
Table 2.2 C The Two Step Production of Hydrogen Peroxide using Anthraquinone 15
Table 2.2 D The Two Electron Oxygen Reduction Reactions 15

Table 3.3 A Summary of Tested MEAs 43

Table 4.1 A MEA I2 Liquid Electrolysis Results 47

Table 4.2 A Vapor Electrolysis Results at Ambient Temperature 49
Table 4.2 B Vapor Electrolysis Results at Elevated Temperature 50

Table 4.3 A Test result for MEA P3 with He bubbled through H2O2 fed to the cathode and humidified air fed to the anode 54
Table 4.3 B Test results for MEA I2 with humidified air feed to the cathode and He bubbled through H2O2 feed to the anode 55

Table 4.4 A Surface Carbon Degradation 56

List of Figures

Figure 2.2 A Models for the Substitution of Carbon by Nitrogen Atoms at the Edges of the Carbon Sheets (Boehm et al., 1984) 18
Figure 2.3 A Sulfuric Acid Analog of Polymer Electrolyte (Sulfuric Acid Model) 19
Figure 2.3 B Chemical Structure of Nafion® (Zhou, et al 2007) 21
Figure 2.3 C Reverse micellar Cluster-Network Structure of Hydrated Nafion® 22
Figure 2.3 D Proton Diffusion via (a) en masse or vehicle and (b) Grotthuss Mechanism. 23
Figure 2.3 E Sample Proton Exchange Membrane Fuel Cell Schematic (Lister & McLean, 2004) 24
Figure 2.3 F Graphical representation for the oxygen concentration over time (Fujita, Nakamura & Muto, 1985) 26
Figure 2.3 G Change in voltage of the PEM Fuel Cell over time (Fujita, Nakamura & Muto, 1985). 27
Figure 2.3 H Schematic view of the 25 cm2 cell for oxygen extraction (Eladeb et al., 2012) 29
Figure 2.3 I Current Density vs. Air Flow (Eladeb et al., 2012). 30
Figure 2.3 J Current Density vs. Cell Voltage (Eladeb et al., 2012) 31
Figure 2.3 K Current Density vs. Time (Eladeb et al., 2012) 31
Figure 2.3 L O2 Outlet Flow vs. the Inlet O2 Flow over Current (Eladeb et al., 2012) 32
Figure 2.3 M Current Density vs. the ORR efficiency (Eladeb et al., 2012) 33
Figure 2.4 A Schematic of dissociation and solvation of the pendant OH- groups within the pores of a hydrated AEM (Grew et al., 2010) 35
Figure 3.1 A Electrolysis Aided PEM Pump Model 38
Figure 3.1 B Two Electron Oxygen Reduction Reaction PEM Pump 39
Figure 3.2 A Example Schematic of Experimental Procedure 40
Figure 3.2 B Diagram for the fuel cell where the cathode is receiving the humidified inlet while the anode is receiving a dry inlet. In addition, the fuel cell is connected to the power supply and the Fuel Cell Test System 40
Figure 3.2 C Overall Diagram of the Fuel Cell Test bed located in the Fuel Cell Center at Worcester Polytechnic Institute 41
Figure 3.2 D HP power supply used for the experimental runs 42
Figure 6.1 A Overview of different electro catalysts for H2O2 production (Siahrostami et al., 2013) 59
Figure 6.3 A Sample Fuel Cell Stack (Fuel Cell Store, 2013) 61
Figure 6.4 A Sample Anion Exchange Membrane for metal cation-free alkaline fuel cell 62
Figure 6.5 A Geometry of a proton exchange membrane (PEM) modeled in COMSOL Multiphysics. (COMSOL Multiphysics, 2014) 63

Abstract

Oxygen transport through a proton exchange membrane (PEM) fuel cell was examined with the ultimate goal of creating a model for a portable oxygen generator. Water electrolysis by four electron oxygen reduction (ORR) along with two electron ORR were tested using membrane electrode assemblies (MEAs) with Pt/C, carbon (Printex L6), and PtIrB catalysts. Results in trials for all configurations yielded small currents and little to no oxygen production. Based on this study, it appears a vapor electrolysis PEM fuel cell oxygen pump and two electron oxygen reduction based on Pt/C and Printex L6 are not feasible. Alternative catalysts for two electron oxygen reduction on a PEM and alternative membranes may lead to more functional models of the proposed electrochemical oxygen generator.

1. Introduction

There are numerous diseases and conditions that affect the respiratory system. While these conditions vary in severity, they all affect those living with these conditions in their everyday lives. Current solutions to respiratory problems, from portable oxygen tanks to oxygen concentrators, can be large, heavy, inconvenient, and can cause potential safety hazards. A new design for a personal and portable device was based on PEM fuel cell. Membrane electrode assemblies (MEAs) would be used as a means to output an enriched oxygen stream that could be delivered directly to the person.

The process is based on the oxygen reduction reaction (ORR). ORR would occur at the cathode while oxygen evolution would occur at the cathode, meaning the anode exhaust would be the oxygen enriched stream. There are two types of ORR, the four electron reaction and the two electron reaction. The four electron ORR reacts via water electrolysis, while the two electron ORR uses hydrogen peroxide as an intermediate. The two electron ORR is preferable to the four electron due to the lower energy costs associated with the reaction.

When considering the MEA, there are two possible ion exchange membranes that could be used in this design: the proton exchange membrane (PEM) and the anion exchange membrane (AEM). The key difference between the two membranes is that the PEM facilitates the exchange of protons across the membrane while the AEM facilitates the exchange of anions across the membrane. Both membranes have advantages to their respective use in this design, however given the established research on PEMs and the relative infancy of AEMs, the PEM was chosen for the MEAs to be used in this study.

Oxygen extraction has been accomplished using PEM electrolysis in some studies (Eladeb et al., 2012), although this study was performed using liquid electrolysis as opposed to vapor electrolysis, which is the ultimate goal of this design. It is important to compare these liquid electrolysis results with the gathered vapor electrolysis results to assess the validity of the vapor PEM electrolysis and its viability as an oxygen pump.

Experimental trials consisted of varying feeds, temperature conditions, and applied voltages to the MEA being tested. A schematic of the experimental system can be seen in Figure 3.2A. Three sets of Nafion® 115 membranes were used with differing catalysts: Pt/C catalyst at both the cathode and the anode, Printex L6 carbon catalyst at the cathode and Pt/C at the anode, and Pt/C at the cathode and unsupported PtIrB at the anode. The voltage was set given the type of ORR being pursued in the trial, voltages lower than 1.2 V being for the two electron ORR while higher voltages were intended to induce the four electron ORR.

The experimental results proved that the initial goal of designing an oxygen generator had been unsuccessful. Neither the Pt/C catalyst nor the Printex L6 catalyst was successful in fostering the two electron ORR in the system. The MEAs loaded with the PtIrB, which were intended for the vapor electrolysis trials, also failed to yield promising results. With little to no observable oxygen evolution at the anode and very small sustainable current through the cell, it would appear that vapor electrolysis is not an efficient method for the transport of oxygen through PEM.

At the conclusion of this study, it was determined that none of the proposed designs as tested in these experiments would yield any kind of practical and efficient oxygen generator

device. Pt/C and Printex L6 catalysts failed to facilitate any two electron ORR across the membrane. Any attempt to further the two electron ORR study using a PEM must be done with alternative catalysts that show more activity for the two electron reaction. Vapor electrolysis did not yield promising enough results to warrant further examination into this method. The low current densities observed along with the mass transport limitations of the system show that the scale up of this system is not worth pursuing.

It is recommended that any further study on this design focus on promoting the two electron ORR for oxygen transport across the PEM. There is the potential for other catalysts to be more active for the two electron ORR, which could potentially lead to a more practical design and a usable model. Oxygen transport using AEM may possibly yield more favorable results, however more research must first be performed on the subject. COMSOL Multiphysics, a physics modeling software, could potentially be used by researchers to perform theoretical calculations and model the MEA before performing future experiments.

2. Literature Review

2.1 Social Implications

There are a number of activities in society that people perform for personal and professional reasons that have a negative effect on the respiratory system when performed repeatedly over long periods of time. The most common way people damage their respiratory system is smoking tobacco. Additionally, there are several materials used in industry that can cause lung damage to those who work with the raw materials and those who use the final product. All of these everyday activities can lead to numerous respiratory diseases and conditions. Finally, air pollution causes respiratory ailments.

2.1.1 Diseases and Conditions

There are a variety of diseases and conditions that affect the respiratory system. According to the UCSF Medical Center, these ailments are divided into four categories; 1) occupational lung diseases which are caused by long term inhalation of industrial irritants such as beryllium, silica, and asbestos; 2) chronic obstructive pulmonary disease (COPD), which is primarily caused by years of tobacco smoking and includes the disease emphysema, which is the fourth leading cause of death in the USA; 3) non-tuberculosis mycobacteria (NTM) which is caused by a group of bacteria normally found in soil and water, and 4) interstitial lung disease (ILD) the causes of which are mostly unknown (UCSF Medical Center, 2002). All of these ailments damage the lung so that it cannot absorb the required amount of oxygen from the air into the blood stream. As such, part of the treatment for these diseases is oxygen therapy, which is quite simply to provide higher concentrations of oxygen to the patients so that their lungs can absorb the necessary amount of oxygen. Oxygen therapy is tailored to the individuals exact condition so that the amount of oxygen supplied varies from cases to case and can be anything from 30% to

98% oxygen. Duration can be for short term use in some cases such as lung infections in which the lungs will generally recover, but the majority of patients on oxygen treatment are on it for the rest of their lives (UCSF Medical Center, 2002).

2.1.2 Current Solutions

There are 3 major ways in which oxygen is stored or generated for such medical use. In hospitals, where the demand for oxygen is high, it is stored in liquid form in chilled tanks. In smaller medical facilities and for home use oxygen is stored in compressed gas cylinders. The large oxygen cylinders can hold 6,500 standard liters of oxygen which will last about 2 days and the smaller portable oxygen cylinders hold 164 or 170 liters and last four to six hours. The last method is to generate oxygen with a personal oxygen concentrator which eliminates the need for storage and regular deliveries of bulk oxygen cylinders. Personal oxygen concentrators for medical purposes most commonly produce oxygen by removing nitrogen from the air via nitrogen adsorption. In this process there are two steps; first nitrogen is adsorbed onto a packed zeolite bed at high pressure, providing an enriched oxygen air exhaust. The second step is to purge the bed of nitrogen by dropping the pressure to below atmospheric pressure (Gauthier, Hendricks & Babcock, 1980). The currently available personal portable oxygen concentrators work on this principle. They are priced around $3,000 – $4,000 and are generally the size of a large laptop bag or small backpack and they can be used in portable application. Most of them have the option of providing ether a continuous flow of O_2 enriched air or else give a periodic pulse of pure oxygen. However, they only have an average battery life of 2.5 – 3 hours, with a few models offering extended battery life at the expense of the weight and size.

In 1995, Ma and Yu (1995) published a paper on a novel electrochemical oxygen concentrator designed for medium scale use in less developed areas. The device produced 36 L of 99.5% pure O_2 an hour. This was achieved through a 2 electron Oxygen Reduction Reaction (ORR) mechanism resulting in oxygen being pumped from the cathode to the anode. The overall reactions at the electrodes and the complete cell are provided in Table 2.1A. In the first reaction air and electricity are fed to a carbon cathode where O_2 is reduced to a hydro peroxide ion. Next the hydro peroxide ion is decomposed on a $Mn(NO_3)_2$ $6H_2O$ mesh to produce oxygen and hydroxide. The resulting hydroxide is then transferred through the 7 M KOH electrolyte to a nickel mesh anode where it is oxidized to produce oxygen (Ma & Yu, 1995).

Table 2.1 A The Half Reaction and Overall Reaction for MA's O2 Concentrator (Ma & Yu, 1995)

Cathode Reaction	O_2 (air) + H_2O + $2e^-$ → HO_2^- + OH^-	Eq 1
$Mn(NO_3)_2$ $6H_2O$ mesh Reaction	HO_2^- → ½ O_2 + OH^-	Eq 2
Anode Reaction	2 OH^- → ½ O_2 + H_2O + $2e^-$	Eq 3
Overall Reaction	O_2 (cathode) → O_2 (Anode)	Eq 4

This provides an attractive alternative to other forms of oxygen production. When compared to the traditional method of oxygen generation, water electrolysis, there are many advantages. The first of which is a lower power requirement; Ma's device uses a 2 electron ORR which theoretically only requires 0.48V along with 2 e^- consumed by the O_2 being pumped, whereas water electrolysis requires higher than 1.23V. Despite the lower energy consumption, the O_2 production remains equivalent to that in water electrolysis. Additionally this method does

not consume water. This system has reportedly been used in several hospitals in China with no reduction in performance after 12 months of continuous use (Ma & Yu, 1995).

2.2 Chemistry

The ORR is a reaction in which O_2 gains electrons (e^-). Oxygen reduction in aqueous solution generally proceeds by one of two routes, a four e^- or a two e^- pathway. These reactions are already widely used in electrochemistry for power generation and H_2O_2 production.

2.2.1 Four Electron Oxygen Reduction Reactions

The 4 e^- ORR is most commonly used for power generation, via a fuel cell. The overall reactions for four e^- ORR in acidic and alkaline electrolyte can be seen in Table 2.2A. These reactions are not spontaneous, comprise several steps, and generally require a catalyst. Many different catalysts have been used and even more are being researched. Among these current and developing catalysts are noble metals, carbon materials, quinone and derivatives, and several transition metal compounds (Song & Zhang, 2008). However, the most common catalyst used commercially today is Pt supported on carbon.

Table 2.2 A The Four Electron Oxygen Reduction Reactions

In Acidic aqueous solution	$O_2 + 4H^+ + 4e^- \rightarrow H_2O$	1.229 V
In Alkaline aqueous solution	$O_2 + H_2O + 4e^- \rightarrow 4OH$	0.401 V

The reverse reaction of the 4 e^- ORR is involved in water electrolysis, as seen in Table 2.2B. Water electrolysis is the simple process of running a sufficient current through water to produce hydrogen and oxygen. This is important to note for the purposes of our paper as this sets the upper limit of our own study. Additionally, it tells us that if we proceed through the four e^- ORR

we will produce hydrogen as well as oxygen, a rather undesirable outcome due to the explosive nature of hydrogen.

Table 2.2 B Water Electrolysis

$2\ H_2O \rightarrow 2\ H_2 + O_2$	1.229 V

2.2.2 Two Electron Oxygen Reduction Reactions

Hydrogen peroxide is very important in industry as an effective and clean way to purify waste water. For this reason, ways of improving hydrogen peroxide production are constantly under study. Currently there are two primary methods of hydrogen peroxide generation. The older method is the electrolysis of aqueous solutions of H_2SO_4, $KHSO_4$, or NH_4HSO_4. More commonly hydrogen peroxide is produced through the hydrogenation, reduction, and then oxidation of anthraquinone derivatives, as seen in Table 2.2C. This is an efficient production method as only hydrogen, atmospheric oxygen, and water are consumed (D. Considine (Ed.), 1974). However, an electrochemical method (Assumpcao et al, 2012) would have two primary advantages over the anthraquinone method. Mainly that it would take less energy to acquire protons from an acidic solution rather than generate H_2 separately. Additionally it is believed that an electrochemical method would be able to achieve a higher efficiency than the 90% conversion rate that the anthraquinone method yields (Panizza & Cerisola, 2008).

Table 2.2 C The Two Step Production of Hydrogen Peroxide using Anthraquinone

Step 1	$C_6H_4:(CO)_2:C_6H_3R + H_2 \rightarrow C_6H_4:(COH)_2:C_6H_3R$
Step 2	$C_6H_4:(COH)_2:C_6H_3R + O_2 \rightarrow C_6H_4:(CO)_2:C_6H_3R + H_2O_2$

More recently the electrochemical generation of hydrogen peroxide has received greater attention. The electrochemical generation of H_2O_2 utilizes the 2 e^- ORR as can be seen in Table 2.2D. To produce H_2O_2 one needs a catalyst that will only reduce oxygen partially, otherwise the H_2O_2 will be further reduced to water. Carbon is believed to be one of the best catalysts for this reaction due to its large surface area, corrosion resistance, and low price. However carbon has many forms which possess a large range of varying properties (Sudoh, Kitaguchi, & Koide, 1985).

Table 2.2 D The Two Electron Oxygen Reduction Reactions

In Acidic aqueous solution	$O_2 + 2H^+ + 2e^- \rightarrow H_2O_2$	0.70 V
	$H_2O_2 + 2H^+ + 2e^- \rightarrow 2\ H_2O$	1.76 V
In Alkaline aqueous solution	$O_2 + H_2O + 2e^- \rightarrow HO_2^- + OH^-$	–0.065 V
	$HO_2^- + H_2O + 2e^- \rightarrow 3OH^-$	0.867 V

Soltani et al. (2012) have explored the idea of generating hydrogen peroxide in situ by electrochemical means. For their experiment they used an undivided cell with a Pt anode and a gas diffusion cathode (GDC), through which they feed oxygen at a rate of 1 L/min. They tested several forms of carbon catalysts coated onto the GDC; including carbon black(CB) –PTFE, powdered activated carbon(PAC) –PTFE, carbon nano tube(CNT)-PTFE, and CB-CNT-PTFE. After a run time of 40 minute with an applied current of 200 mA they found that the CB-CNT-PTFE (123.5

μM) did the best and the PAC-PTFE (58.45 μM) did the worst. However, because the CB-PTFE (112.3 μM) and CNT-PTFE (100.9 μM) preformed similarly and costs significantly less than the CB-CNT-PTFE, they used the CB-PTFE as their catalyst for all subsequent experiments (Soltani et al., 2012).

In addition to testing for an effective catalyst, they also tested the effects of initial pH, electrolyte concentration, and applied current on the generation of hydrogen peroxide. They tested initial pHs between pH 2 – pH 9 and found the best conditions were at pH 3 and above pH 7. Above pH 7 the hydrogen peroxide primarily exists as the hydroperoxide ion, which is stable in basic solution. On the other hand, acidic solutions tend to reduce the hydrogen peroxide to water and the catalyst will facilitate the formation of H_2 from acidic protons in the solution. Next these investigators examined H_2O_2 generation at different electrolyte concentrations. They used Na_2SO_4 as there electrolyte and applied 300 mA to a range of concentrations: 0.01, 0.03, 0.05, 0.08, 0.1, and 0.15 M. They found that higher electrolyte concentrations lead to more H_2O_2 with insignificant increases over 0.08 M. They also tried a range of applied currents from 30 mA to 300mA. Once again they found that increased current resulted in increased H_2O_2 production up to 150 mA after which the increase in H_2O_2 concentration was insignificant. Finally Soltani et al. notes that after ten 70 minute runs there is a slight decrease in the performance of their cell, though they do not speculate why (Soltani et al., 2012).

Assumpcao et al. (2012) did a direct comparison of two types of carbon; Printex L6 and Vulcan XC 72R. They found that Vulcan XC 72R transferred an average of 2.9 electrons per molecule and produced 51% H_2O_2. This is not particularly surprising as Vulcan XC 72R is one of the most common carbon supports used in modern fuel cell catalysts in which noble metals are

loaded onto carbon supports. On the other hand, they found Printex L6 transferred an average of 2.2 electrons per molecule and produced 88% H_2O_2. To determine why there was such a difference between these two carbons they looked at the composition of each. They found sulfur, oxygen, and nitrogen in both carbons, with the majority of it appearing as oxygenated acids. Additionally the Printex had more than two times the oxygenated acids compared to the Vulcan. As more oxygenated acids increases the hydrophilicity of the carbon and this facilitates the formation of H_2O_2, it is believed that this is the main reason for the difference in H_2O_2 production (Assumpcao et al, 2012).

Boehm et al. (1984) has also explored the effectiveness of carbon as a catalyst for ORRs. Their group looked at 4 forms of carbon and several methods of pretreatment. The 4 forms of carbon are: Peat charcoal, wood charcoal, sugar charcoal, and carbon black. Each catalyst was tested in the oxidation reaction of dilute sulfuric acid by O_2. It was found that peat charcoal was a good catalyst, wood charcoal was a poor catalyst, and carbon black and sugar charcoal showed little to no activity. Next the catalysts were subjected to heat treatment before testing. It was found that heat treatment increased the activity of all the catalysts, with optimal temperature treatments being 1070K for the charcoals and 1170K for the carbon black. Additionally surface treatments where evaluated. Generally, basic surface oxidants where found to slightly increase the activity of the catalyst and acidic surface oxidants decreased the activity of the catalyst. However, treatment with ammonium at elevated temperatures was found to dramatically increase the catalysts activity. It is believed that heat treatment with ammonium resulted in Nitrogen being incorporated into the outer layers of the carbon catalyst, as seen in Fig 2.2A. The Nitrogen in the carbon structure increases the activity of the catalyst by giving its extra electrons

to the conduction band which in turn gives its electrons to the adsorbed molecules, making the carbon atoms adjacent to the nitrogen atom more active (Boehm et al., 1984).

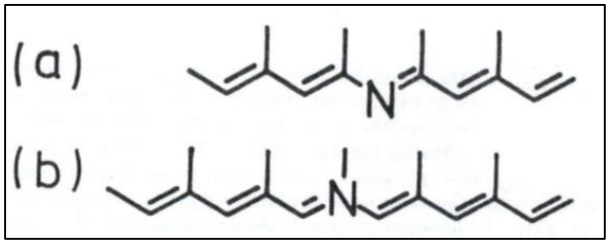

Figure 2.2 A Models for the Substitution of Carbon by Nitrogen Atoms at the Edges of the Carbon Sheets (Boehm et al., 1984)

2.3 Proton Exchange Membrane (PEM)

2.3.1 Introduction to PEMs

Since the proposed device is based on a PEM fuel cell, a background is provided here. Proton electron membranes (PEM) were first seen in the 1960s within fuel cells as auxiliary power source in the Gemini space flights (Lister & McLean, 2004). Stanley H. Langer and Robert G. Haldeman of American Cyanamid Company were able to subsequently successfully use them to purify oxygen using 11.2 mg/cm^2 of Pt on a stainless mesh screen as the electrode, while electrolyte was simply 5 disks of filter paper saturated in 23% of KOH solution (Langer & Haldeman, 1964). Their experimental work was the ground-work for proving that four-electron mechanisms are operative and feasible in oxygen pumping. In addition, their work provided a basis for other studies to be conducted such as catalytic materials and oxygen electrode mechanisms. However, major advances in terms of redesign and configuration of PEM fuel cells did not occur till the 1980s. Researchers have constantly been looking to enhance the design and have succeeded by trying to reduce the expensive platinum catalyst to finding alternative catalysts.

2.3.2 Mechanism

Proton exchange membranes are a type of semipermeable membranes designed to conduct protons whiles the membranes tend to be impermeable to gases such as hydrogen or oxygen. PEM fuel cells are based off the normal membrane electrode assembly (MEA), whose basic function involves hydrogen oxidation at the anode, OOR at the cathode anode and transfer of protons through the PEM.

The early electrolytes were aqueous solutions of acids and bases. To reduce the Ohmic resistance, these could be soaked on a thin porous disk or on a membrane. The basic concept of the polymer electrolyte involves covalently binding the acid group to a polymer in the form of a membrane rather than immobilizing the liquid acid electrolyte within a porous support layer that is held there physically via capillary and surface forces so that leaking of the acid is avoided. Thus, this concept avoids the dissolution, volatility, and migration acid electrolytes altogether. To better understand this PEM concept, it has been exemplified schematically for the case of sulfuric acid in Figure 2.3A, where one of the –OH groups in sulfuric acid is replaced by a polymer chain R, resulting in a solid polymer electrolyte with a sulfonic acid group, i.e., R–SO3H.

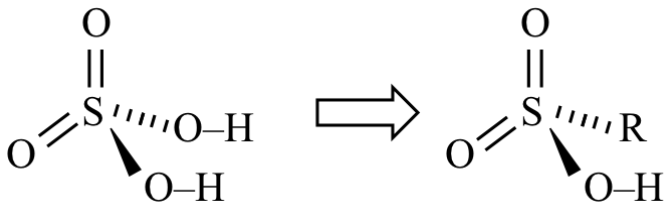

Figure 2.3 A Sulfuric Acid Analog of Polymer Electrolyte (Sulfuric Acid Model)

When such a polymer electrolyte, also called ionomeric polymer, or simply an ionomer, is brought in contact with water, hydronium ions, or hydrated protons, are formed by the following reaction:

$$R - SO_3H + H_2O \leftrightarrow H_3O^+ + R - SO_3 \quad (2.3.1)$$

The reaction facilitates conduction of protons to occur in the aqueous phase. Thus, the polymer electrolyte acts like an ordinary acidic electrolyte, except that not only does it anchor the acid group, the resulting anion is not solvated, and thus does not participate in conduction, which is carried out solely by the hydronium ions. Of course, anions and hydronium ions in PEM must stay close together to maintain overall electrical neutrality within the ionomer. These two conditions can be satisfied only if micelles or reverse micelles are formed, with water and the polymer as the continuous phase, respectively. Thus, reverse micelles, or inverted micelles, are formed when water is introduced into PEMs, as for example in Nafion®.

In principle, the polymer chain R may be selected from a wide range of possible options and, hence, a number of different PEM materials have been investigated. In practice, R must be electrochemically and thermally stable and should preferably be hydrophobic and/or cross-linked to avoid excessive swelling in water (Mauritz & Moore, 2004). The early polymer electrolytes developed were blends of polymer with a highly cross-linked polystyrene-based ionomer. However, these materials were found to not possess adequate chemical stability under the harsh oxidative environment in an operating fuel cell, because of the instability of the C–H bond in the polymer. A stable ionomer with excellent conductivity was found in 1962, when DuPont developed the Nafion® membrane, which is based on a highly chemically inert backbone structure similar to PTFE, as shown in Figure 2.3B. The chemical inertness of Nafion® is due to the fact that the C–F bonds in it are much more stable than the C–H bonds present in the hydrocarbon-based membranes (Coms, 2008).

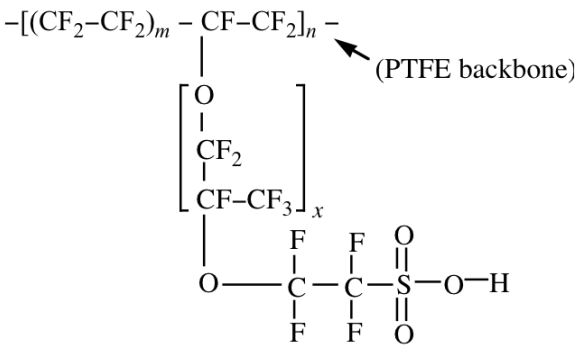

Figure 2.3 B Chemical Structure of Nafion® (Zhou, et al 2007)

The molecular mass (weight) of Nafion® depends upon *m* (5-13), *n* (~1000), and *x* (0-3) (Figure 2.3B), and is typically in the range of 105 – 106 Da. The properties that are typically used to characterize Nafion® membranes, however, are the equivalent weight (EW) and the membrane thickness. The EW is defined as the number of grams of dry Nafion® per mol of acid groups. Thus, it is essentially the molecular weight (Da) of the anion –RSO3−. A typical value for Nafion® is 1100.

In fact, a Nafion® membrane is denoted by a number in which the first two digits represent its EW, while the last denotes its nominal thickness. Thus, Nafion® 117 is a membrane with an EW of 1100 and a nominal thickness of 0.007 in (178µm). Other common membranes are Nafion®115 (0.005 in. or 125µm) and Nafion® 112 (0.002 in. or 50µm) (Sigma Aldrich). While a thinner membrane can provide better fuel cell performance due to lower resistance, it is less durable than a thicker membrane and has a higher permeability to O_2 and H_2, resulting in more crossover.

The PFSA backbone is strongly hydrophobic, while the proton conducting sulfonic acid group is highly hydrophilic and, thus, phase separation readily occurs when water is introduced into the Nafion®, forming interconnected aqueous reverse micelles or clusters, roughly 4 nm in size and interconnected by channels of roughly 1 nm size responsible for percolation, that contain water, the anion, and the hydronium ions, as shown in Figure 2.3C, (Personal Notes by Prof. Datta).

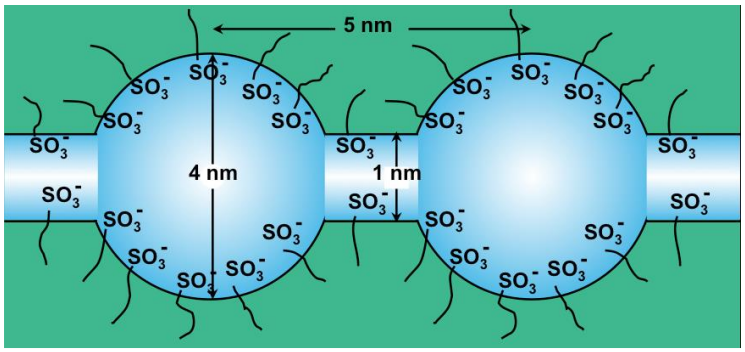

Figure 2.3 C Reverse micellar Cluster-Network Structure of Hydrated Nafion®

By minimizing the interfacial area, the spherical shape for clusters or inverted micelles ensures minimum energy of interaction between the hydrophobic and the hydrophilic regions.

Another interesting aspect of these membranes is the anomalously high conductivity of hydronium ions. For instance, at 25 ºC, λ_{10} = 349.8 S.cm^2/equiv in water, which is extremely high when compared with equivalent conductivity of other cations of size similar to the hydronium ion, e.g., Na_+. In other words, the conductivity cannot be accounted for simply by the hydrodynamic vehicular diffusion, in which the hydronium ion diffuses *en masse*, as modeled, for instance by the Stokes-Einstein model. The difference can be explained by an unusual mechanism known as the Grotthuss (or structural) mechanism of proton diffusion that supplements the *en masse* diffusion. It was proposed over two-hundred years ago, prior to the formulation of Fick's law, and imagines that the proton simply hops from the hydronium ion to an adjacent water molecule, becoming a hydronium ion and leaving a water molecule behind, and so on, as shown schematically in Figure 2.3D. The Grotthuss mechanism involves two sequential steps, namely, rotation of the dipolar water molecule due to the electric field of the adjacent hydronium ion into a receptive orientation, followed by the transfer of proton to the water molecule, via quantum mechanical tunneling from hydronium ion. The Grotthuss model of "chain mechanism"

for the transfer of protons in water is ingenious considering that in 1806 the chemical formula of water was not settled, and the concept of molecules was new (Personal Notes by Prof. Datta)..

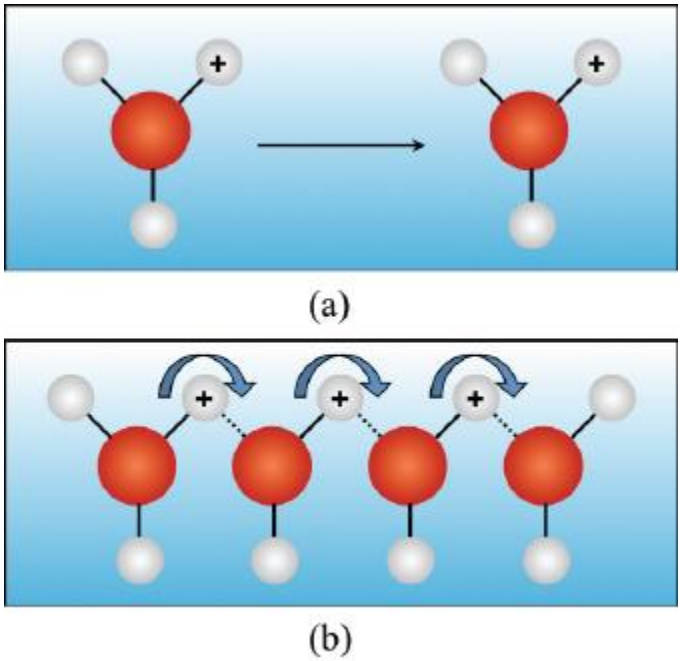

Figure 2.3 D Proton Diffusion via (a) en masse or vehicle and (b) Grotthuss Mechanism.

2.3.3 Hydrogen Oxygen Fuel Cell

The design and structure of fuel cell is described below. The electrode is the layer that sits on each side of the PEM. Therefore, to ensure an effective design, an electrode must provide for the three main transport processes with the fuel cell. These transport processes include protons from the membrane to the catalyst, electrons from current collectors to the catalyst through the gas diffusion layer, and finally the reactant and product gases to and from the catalyst layer and the gas channels. Protons, electrons and gases are known as the three phases that can be found within the electrocatalyst layer. These phases must be correctly spread across the catalyst layer to optimize that electrode design and reduce transport loss. Thus, an effective line plate interface among between phases is needed for the PEM fuel cell to operate effectively.

The PEM is the central piece of the membrane electrode assembly (MEA) and exterior layers on each side together form the electrode. The next layer is the Catalyst Layer as seen in Figure 2.3E sits between membrane and gas diffusion layer (GDL), and is also known as the active layer (Lister & McLean, 2004). The layer is the location where the half-cell electrode reaction takes place in the PEM fuel cell. Adjacent to the catalyst layer, as seen in Figure 2.3E, is the gas diffusion layer whose sole purpose is to ensure reactants diffuse effectively to the catalyst layer and also transports electrons to and from the catalyst layer. In most cases, the layer is made up of porous carbon paper or a graphite cloth, which is roughly 100-300 um thick (Lister & McLean, 2004).

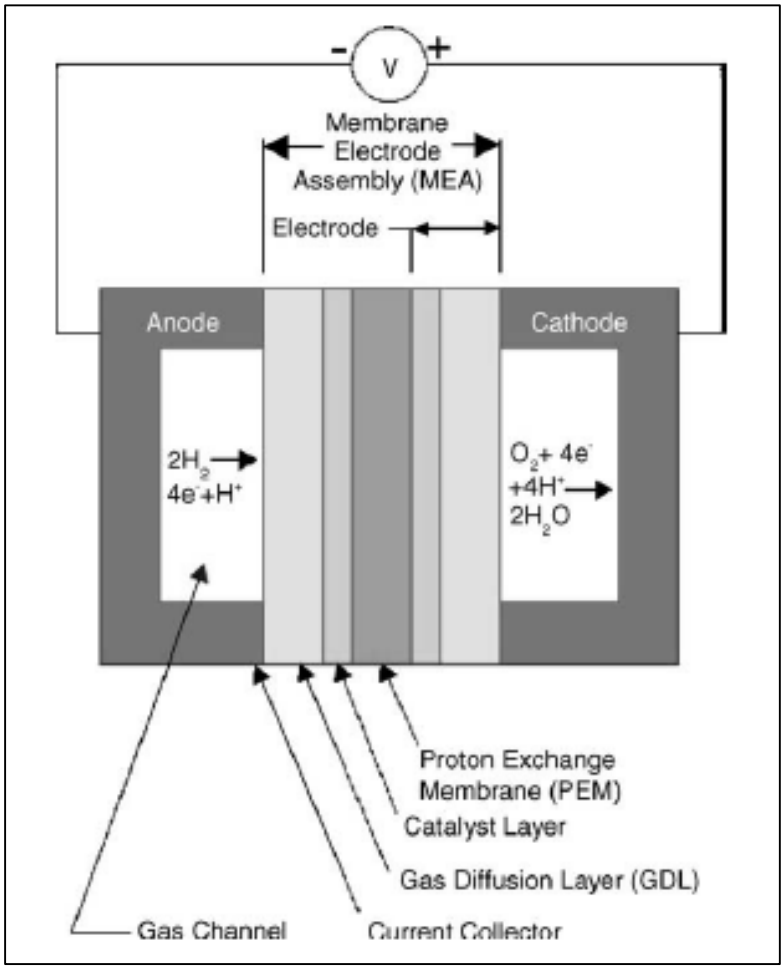

Figure 2.3 E Sample Proton Exchange Membrane Fuel Cell Schematic (Lister & McLean, 2004)

PEMFC is fueled by hydrogen and the charge carrier is the hydrogen ion (H^+). At the anode, the hydrogen molecule is split into hydrogen ions and electrons. These hydrogen ions permeate across the electrolyte to the cathode side. However, the electrons flow through an external path and generate electrical power. Oxygen, usually in the form of air, is supplied to the cathode and combines with the electrons and the hydrogen ions coming above the electrolyte layer to produce water. The reactions at the electrodes are as follows:

Anode reaction: $2H_2 \rightarrow 4H^+ + 4e^-$

Cathode reaction: $O_2 + 4H^+ + 4e^- \rightarrow 2H_2O$

Overall cell reaction: $2H_2 + O_2 \rightarrow 2H_2O$

2.3.4 Oxygen generation case studies

The following section will address many advances in this field of research. Significant advances were not conducted until the 1980s. For instance, Yuko Fujita et al. (1985) conducted a research study on an oxygen separator based on oxygen reduction at the air cathode. This study specifically focused on the previous O_2 separators that used a liquid electrolyte, and that there was little published work on O_2 separators that use a polymer electrolyte membrane. Thus, was one of the first published studies using the Nafion® 117. Pt anode was plated onto the membrane and Pt/C cathode was hot pressed onto the membrane. In addition, the series of experimental testing was conducted on 10 cm^2 and 100 cm^2 active areas. Fujita et al. (1985) found the following parameters which included operating temperature of 40^o C water flowing to the anode and air at STP that flows 4 L/min to the cathode (Fujita, 1985). With this setup, the output of the PEMFC is 70.9 ml/min O_2, with a concentration of 98.4%, and current efficiency of oxygen reduction or ϕ of 91.3%.

The test method was to run on circulation mode in order to remove all O_2 from 1 L of air. It took 70 min to remove all O_2 (final O_2 concentration of 0.02%) as seen in Figure 2.3F. At this scale, in flow through mode, a stream of 0.02% O_2 can be achieved with a flow of 100 ml/min.

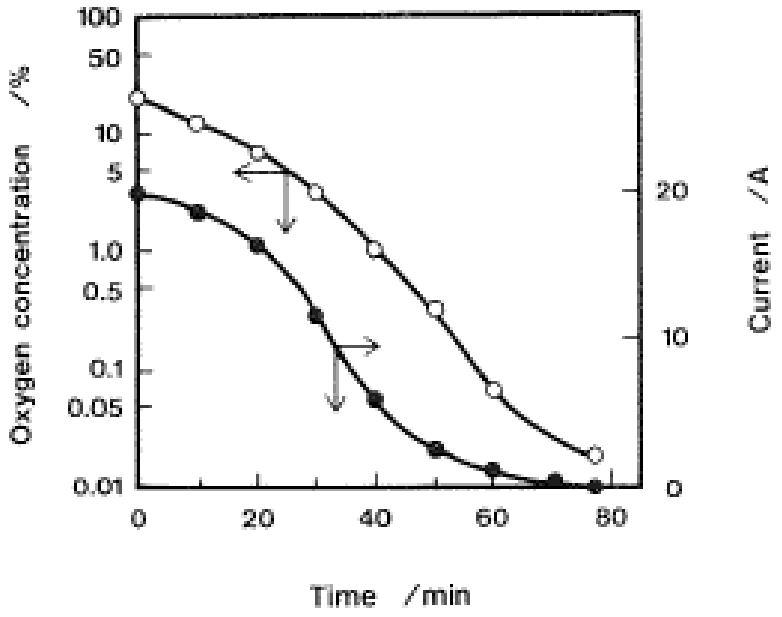

Figure 2.3 F Graphical representation for the oxygen concentration over time (Fujita, Nakamura & Muto, 1985)

Based on the Fujita study, the following conclusions can be made that: (a) water produced at cathode is discarded, (b) water at anode is recycled and (c) air feed is humidified at 40^o C. For longevity tests, Figure 2.3G shows the 100 cm^2 cell was used intermittently for 7.5 hours per day at 200 mA/ cm^2. In addition, the overall design is an effective O_2 separator and includes the following: lower ϕ and Y_{O2} than Takenaka et al (1982), superior O_2 separation than liquid electrolyte systems, no decrease in performance over 100 days as seen in Figure 2.3G and that humidified air doesn't change the cells operation. Additional observations are that humidified air

doesn't flood the cathode and recycling the water from the cathode doesn't seem to build up impurities.

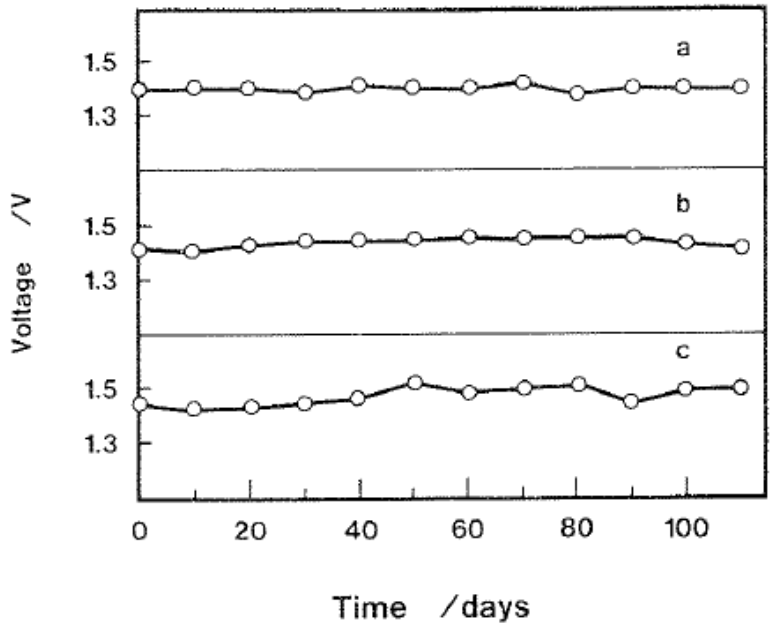

Figure 2.3 G Change in voltage of the PEM Fuel Cell over time (Fujita, Nakamura & Muto, 1985).

Furthermore a more recent study conducted for O_2 separation with PEM technology is described next. The removal of O_2 from the air is important as low O_2 levels help prevent food spoiling, metal corrosion, and are needed for some biological reactors. There are several non-electrochemical ways to lower the O_2 levels: adding N_2, selective O_2 combustion, O_2 selective reduction, selective adsorption, or membrane separation. However, there are more effective electrochemical ways to remove O_2 from air. Winnick (1990) reviewed electrochemical O_2 extraction and Langer & Haldeman (1964) was able to recover pure O_2 from air in alkaline and acidic solutions. The equilibrium voltage of such a cell is 0, but the actual cell voltage is equal to the 2 over potentials, plus the Ohmic drop across the cell. Additionally, General Electrics has recently developed a similar system to provide O_2 from high pressure air. Several patents also

describe processes where O_2 is reduced to O^{2-} and transported through an oxide lattice that is missing oxygens (i.e. a solid oxide conductor). However, the current densities are below 100 mA/cm^2 and the operating temperature is above 500^o C. Tseung & Jasem (1981) imagined O_2 extraction by its reduction to hydrogen peroxide on a graphite based cathode through 2 electron ORR. Brillas et al. (1997), developed a 2 electron reduction path across a membrane using a $NiCo_2O_4$ surface to reform O_2 (current density is limited below 0.2 A/cm^2 by the finite concentration of peroxide). Recently using proton exchange membrane fuel cells (PEMFC), O_2 extraction was reached with current densities of 0.6 A/cm^2 and 0.015 M O_2 per second per m^2 membrane. Based on this information, Eladeb et al. (2012) conducted a series of experiments on PEM fuel cells to garner a better understand on the performance of a PEMFC. Their goal was to remove all O_2 from a stream of air using PEM technology. To achieve this they used a standard water electrolysis MEA, as seen in Figure 2.3H, to reduce oxygen from the inlet stream at the cathode to water. The formed water is then electrolyzed at the anode yielding oxygen, protons, and electrons. The protons are then recycled within the membrane for subsequent oxygen reduction at the cathode (Eladeb et al. 2012).

The MEA was designed for water electrolysis and experiments took place between 50^o and 80^o C. Liquid water was pumped to the anode compartment and heated before entering the cell. The cell was operated at a fixed voltage or controlled current density using a PGSTAT 30autolab potensiostat connected to a 20 amp autolab booster (Eladeb et al., 2012).

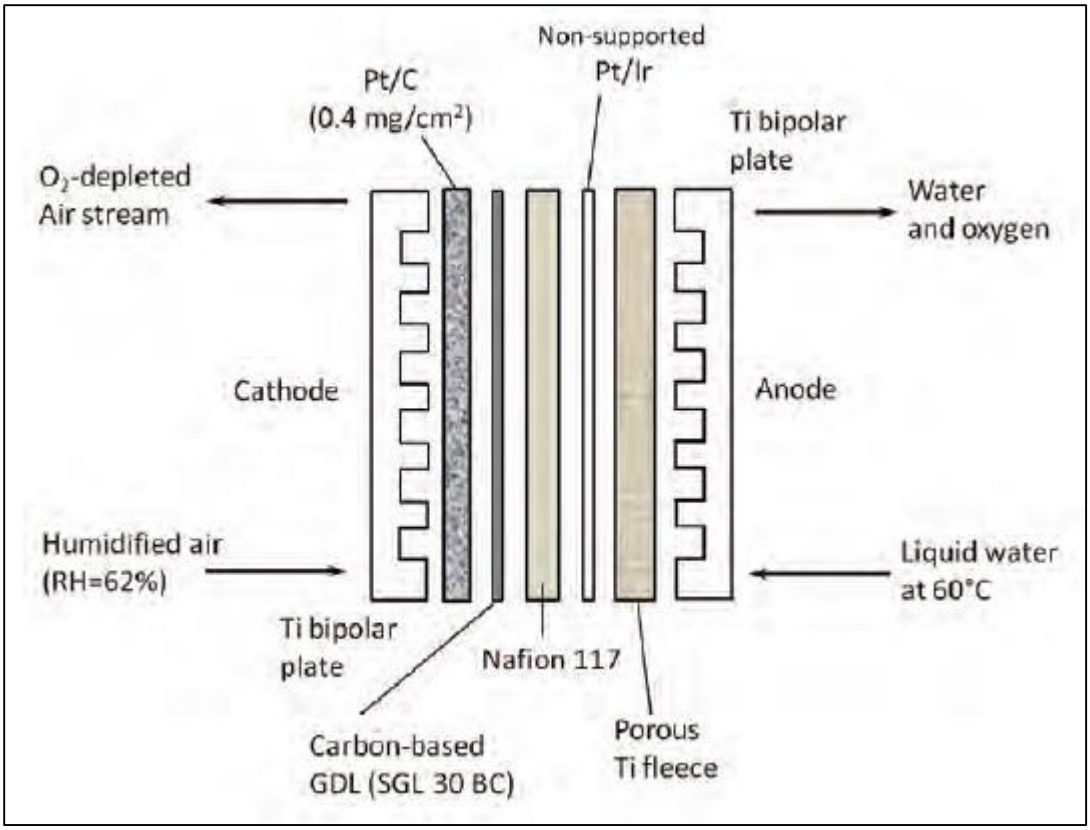

Figure 2.3 H Schematic view of the 25 cm2 cell for oxygen extraction (Eladeb et al., 2012)

The current density vs. voltage was established in either potensiostatic or galvinostatic modes so that the cell potential was below 1.4 v for long runs. Most measurements were carried out with air but O_2 was also used for comparison. O_2 extraction was achieved repeatedly with a fixed current density and cell voltage less than 1.4 v. During most runs in this study the cell voltage stabilized after 10 to 30 minutes. Outlet gas composition was determined with gas chromatography. The following results are for all experimental runs at T = 60°. Figure 2.3I shows that the air flow rate affects the current density at 1.3 v. with the current density increasing with the increase in flow rate (Eladeb et al., 2012).

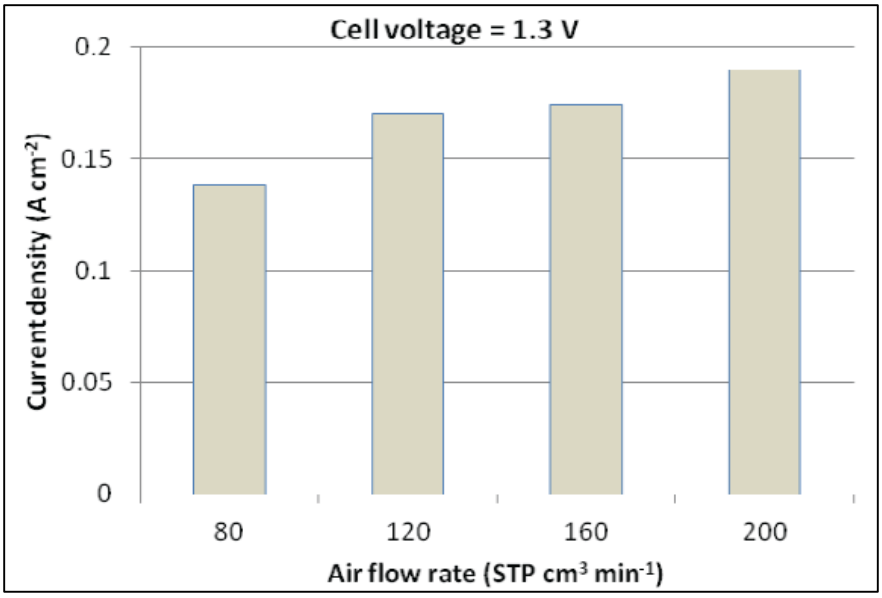

Figure 2.3 I Current Density vs. Air Flow (Eladeb et al., 2012).

Figure 2.3J shows that the cell current density is an increasing function of the voltage. These results are consistent with other research. Voltage and current density are proportional. And we see better efficiency with pure O_2. Figure 2.3K shows the stability of the cell for long runs of up to 50 hours (Eladeb et al., 2012).

Figure 2.3L demonstrates that as inlet O_2 flow increases the outlet O_2 flow approaches atmospheric composition (21% O_2). This is expected and demonstrates the optimal flow rate for the cell (lambda ~ 5-10). Furthermore, this graph indicates that at larger flow rates calculating efficiency of the ORR will be imprecise, as demonstrated in Figure 2.3L. Despite low precision, Figure 2.3L clearly shows a decrease of ORR efficiency as lambda increases. Furthermore, the graph shows that the average ORR efficiency is between 70% and 100% (Eladeb et al., 2012).

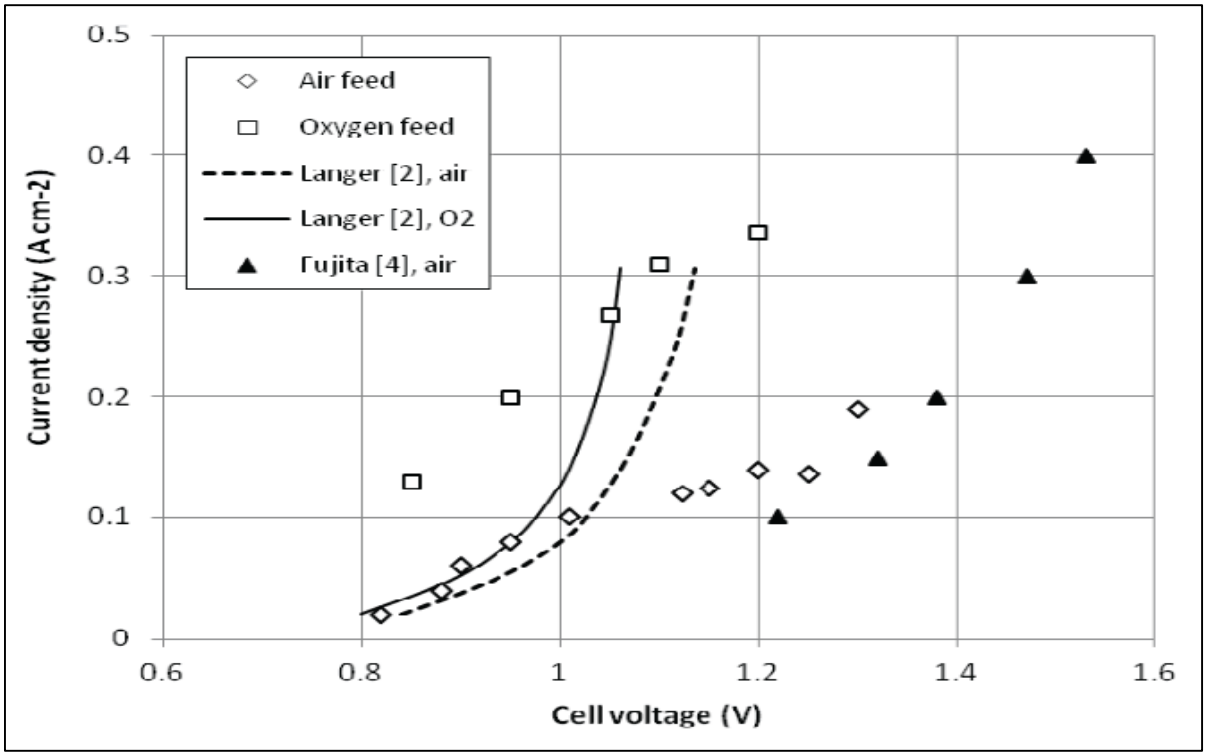

Figure 2.3 J Current Density vs. Cell Voltage (Eladeb et al., 2012)

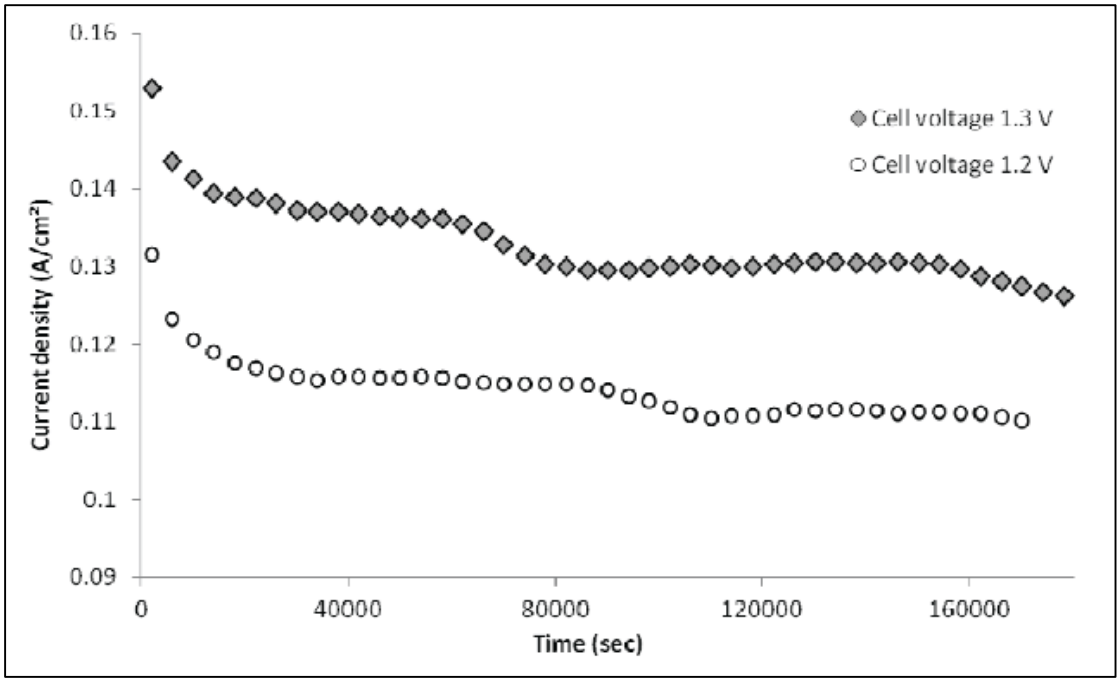

Figure 2.3 K Current Density vs. Time (Eladeb et al., 2012)

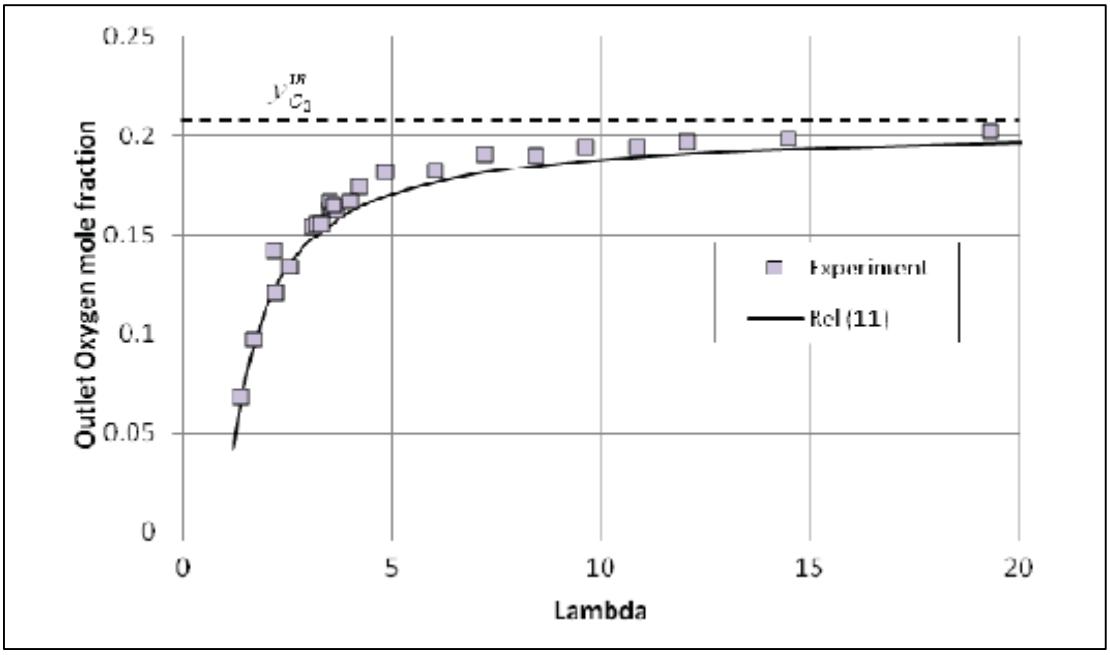

Figure 2.3 L O2 Outlet Flow vs. the Inlet O2 Flow over Current (Eladeb et al., 2012)

Figure 2.3M demonstrates that for current densities of 100 mA/cm^2 or more a 90% or higher ORR efficiency can be observed. The graph shows that current density has a positive effect on ORR efficiency. Thus, this study proves the validity of using water electrolysis in a PEM fuel cell like device for oxygen pumping (Eladeb et al., 2012).

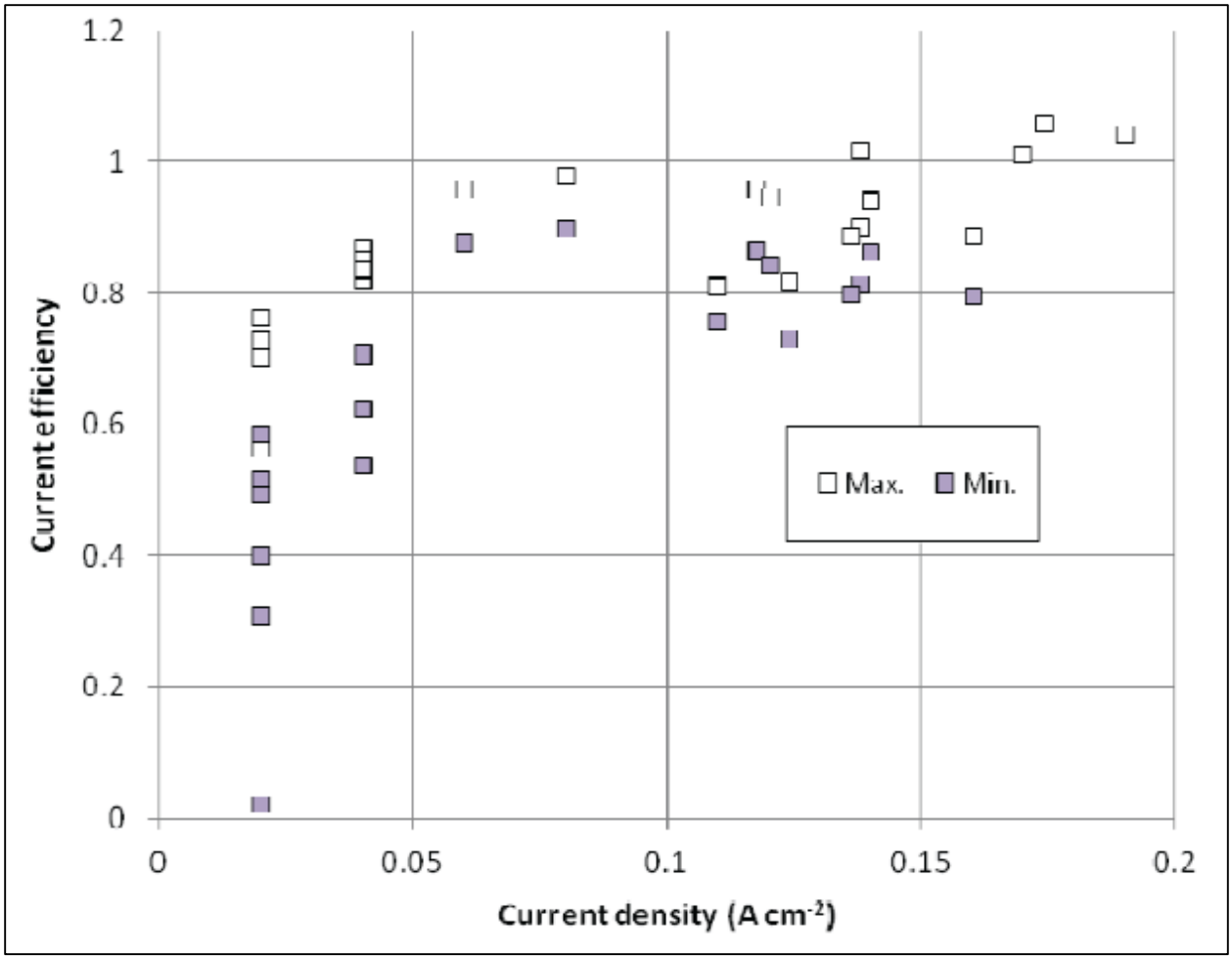

Figure 2.3 M Current Density vs. the ORR efficiency (Eladeb et al., 2012)

2.4 Anion-Exchange Membrane (AEM)

2.4.1 Development

Alkaline fuel cells were developed in the 1930s by F. T. Bacon (Arges et al., 2010). Initial fuel cells used a liquid electrolyte, commonly an aqueous solution of KOH due to its effectiveness as a highly conducting alkaline hydroxide (Merle et al., 2011). These fuel cells suffered from problems due to the use of the liquid electrolyte. The strong alkaline electrolytes result in its reaction with carbon dioxide in air, resulting in the formation of carbonates and the

corresponding reduction of the connectivity of the electrolyte (Arges et al., 2010). This deterioration is discussed further in the subsequent sections.

The recent development of anion exchange membranes has eliminated the need for a liquid electrolyte and promoted the use of an anion exchange membrane as the medium for the transport of hydroxide ions. In these membranes, as in proton exchange membranes, the electrolytes are fixed to polymer chains (Arges et al., 2010). Progress on anion exchange membranes and their use in fuel cells lags behind that of the proton exchange membranes. Commercial production of anion exchange membranes has only begun recently, and research concerning these membranes is currently being conducted. These membranes have proven to resist contamination and maintain ionic conductivity in neutral environments over an extended period of time (Vega et al., 2010). Such studies show that the anion exchange membranes are able to operate at a reasonable level, even in ambient air, and are able to be a viable option to the proton exchange membrane.

2.4.2 Mechanism

An anion exchange membrane consists of a fixed polymer backbone on which electrolytes that have interchangeable anions are attached. Common anion exchange groups in anion exchange membranes are quaternary ammonium, quaternary phosphonium, and tertiary sulfonium (Merle et al., 2011) In the presence of a solvent, these fixed polymers become mobile and are able to transfer charge. Like in a proton exchange membrane, ion transport in an anion exchange membrane occurs via the Grotthuss mechanism. In this mechanism, hydroxide ions are transported through the membrane along a chain of water molecules. The ion moves from one

molecule to another by means of the formation and cleavage of hydrogen bonds as seen in Figure 2.4A, making a tetrahedral water molecule with each bond formed (Merle et al., 2011).

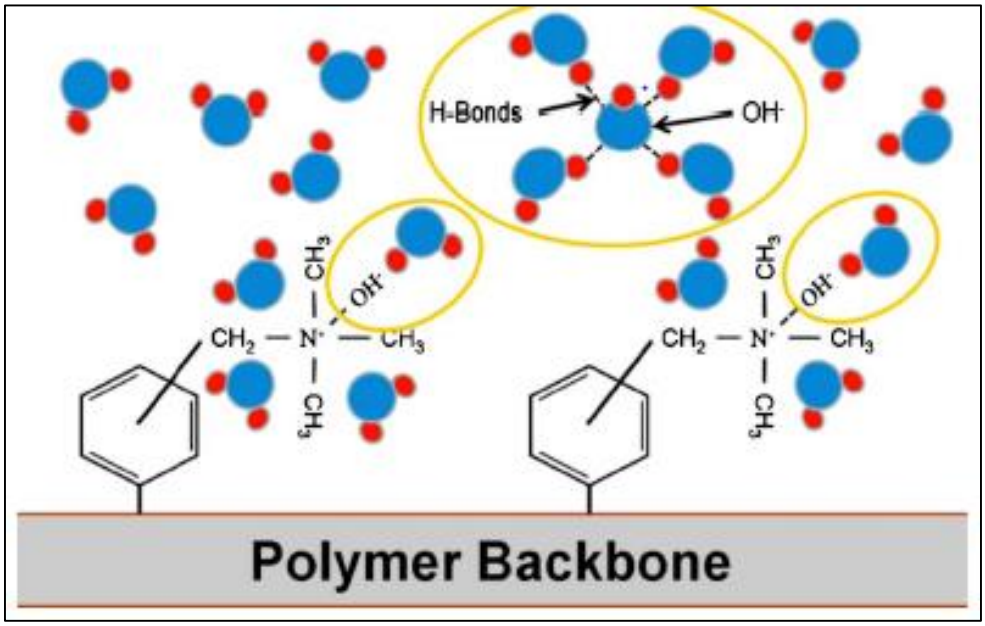

Figure 2.4 A Schematic of dissociation and solvation of the pendant OH- groups within the pores of a hydrated AEM (Grew et al., 2010)

Anion exchange membrane fuel cells function in a very similar way to proton exchange membrane fuel cells. The difference between the two lies in the ions that are transferred between the cathode and the anode. Within the anion exchange membrane fuel cell, hydroxide ions are produced through oxygen reduction at the cathode. This hydroxide ion is carried through the membrane by way of the polymer electrolyte. Upon reaching the anode, the hydroxide ion combines with hydrogen and form water. The electrons that are displaced during the hydrogen oxidation return to the cathode where they participate in the reduction of oxygen that produces the hydroxide ions. The flow of electrons from the anode to the cathode provides the electrical energy that is produced by the fuel cell.

2.4.3 Benefits and Challenges

Anion exchange membranes have numerous advantageous aspects to their use. Among these beneficial qualities are the capabilities of these membranes in fuel cells to operate using a variety of fuels, generate high energy density, and they can be operated at moderate temperatures. One of the largest benefits to using anion exchange membranes is the expensive metal catalysts used in proton exchange membrane fuel cells are not essential for operation. This is due to the higher reaction kinetics at the electrodes in the alkaline conditions of the anion exchange membrane, especially for the oxygen reduction reaction, which translates into a higher electrical efficiency and a lower cost (Merle et al., 2011). This allows either the use of a less expensive catalyst or a lesser amount of the traditional platinum catalyst.

In general, many of the anion exchange membranes benefits are related to the reducing the overall costs of operating a device using an anion exchange membrane. The ability to operate at a lower temperature means less energy is required to maintain the unit at the desired temperature. The ability to use a less expensive catalyst or a smaller amount of an expensive catalyst also lowers the required costs associated with the process. While these benefits have some promising attributes, several problems with the use of anion exchange membranes exist.

One issue with anion exchange membranes include the inability for hydroxide ions to dissociate as strongly as hydrogen ions. While this can be enhanced with the increasing of the number of cationic sites, this method ultimately leads to the deterioration of the membrane itself (Arges et al., 2010). Another problem with the anion exchange membrane is the susceptibility of the hydroxide groups to be neutralized by carbon dioxide. When the membrane is exposed to air, the hydroxide ions are replaced with carbonate and bicarbonate ions (Varcoe et al., 2010), which in turn reduces the pH. The reduction in pH slows the kinetics of the reactions at both the

cathode and the anode, and the larger carbonate and bicarbonate anions cause a decrease in the conductivity of the membrane. This causes a decline in the efficiency and performance of the membrane (Arges et al., 2010).

Another challenge facing anion exchange membranes at this time is the lack of research and development in the area. Of course, this problem will solve itself over time as more research concerning these membranes is conducted. At this time however, anion exchange membranes fall far behind proton exchange membranes in terms of use in membrane electrode assemblies (Arges et al., 2010). In addition, much of the research concerning anion exchange membranes has occurred at the traditional conditions, including the use of expensive catalysts such as platinum. In essence, many of these studies have not taken advantage of the inherent benefits of an anion exchange membrane. Further studies that examine the anion exchange membrane in more appropriate conditions are required to accurately compare the capabilities of the membrane compared to that of the proton exchange membrane in fuel cells.

2.4.4 Oxygen Generation Case Studies

Due to the relatively young age of the anion exchange membrane, there have not been any studies exploring the generation of oxygen using an anion exchange membrane. Considering the research conducted on the generation of oxygen using a proton exchange membrane and the recent developments in developing stable anion exchange membranes, it is very likely that studies exploring this in anion exchange membranes will soon come to light. With the numerous advantages of anion exchange membranes, including the use of cheaper catalysts and the ability to function at lower operating temperatures, anion exchange membranes appear to be a possibly very effective component in oxygen generation.

3. Methodology

3.1 Conceptual Design

As previously discussed in the literature review, there are several applications in the medical field for an oxygen concentrator or an oxygen pump. Current solutions to this problem are both large and inconvenient or contain compressed gas which could potentially be dangerous. For this reason, it was decided to pursue the development an oxygen pump that operates electrochemically using an ion exchange membrane in a fuel cell like device. Given the nascent technology for anion exchange membranes, it was decided to pursue models based on proton exchange membranes.

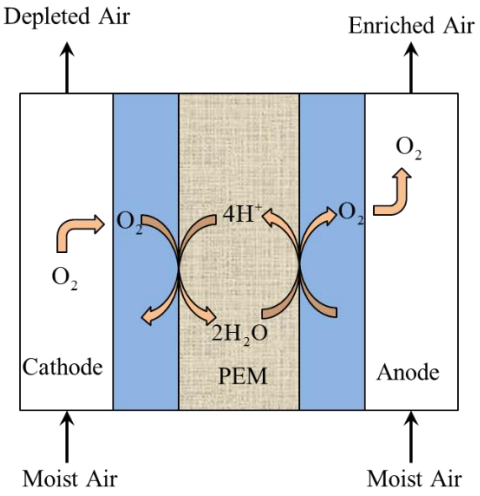

Figure 3.1 A Electrolysis Aided PEM Pump Model

Two potential oxygen pump transport models were conceived. The first model is an electrolysis aided oxygen pump. A schematic of this system can be seen in Figure 3.1A. In this model, oxygen is reduced from the inlet stream at the cathode to water. The formed water is then electrolyzed at the anode yielding oxygen, protons, and electrons. The protons are recycled

within the membrane for subsequent oxygen reduction at the cathode. The oxygen formed at the anode is released in the anode exhaust stream as a part of the oxygen enriched stream.

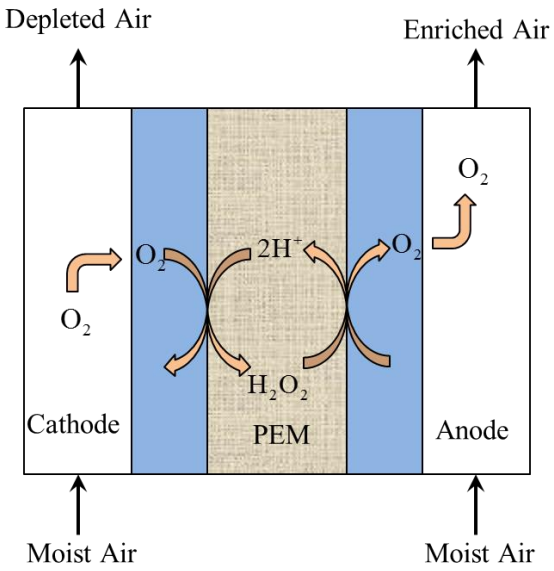

Figure 3.1 B Two Electron Oxygen Reduction Reaction PEM Pump

The second conceptual model for oxygen transport is by way of the two electron oxygen reduction reaction. A schematic of this process can be seen in Figure 3.1B. Oxygen from the cathode inlet is reduced to hydrogen peroxide at the cathode. Hydrogen peroxide is transported through the membrane and is electrolyzed at the anode, yielding oxygen, protons, and electrons. The protons are recycled within the membrane, and the oxygen is released in the anode exhaust stream as part of the oxygen enriched stream.

3.2 Apparatus

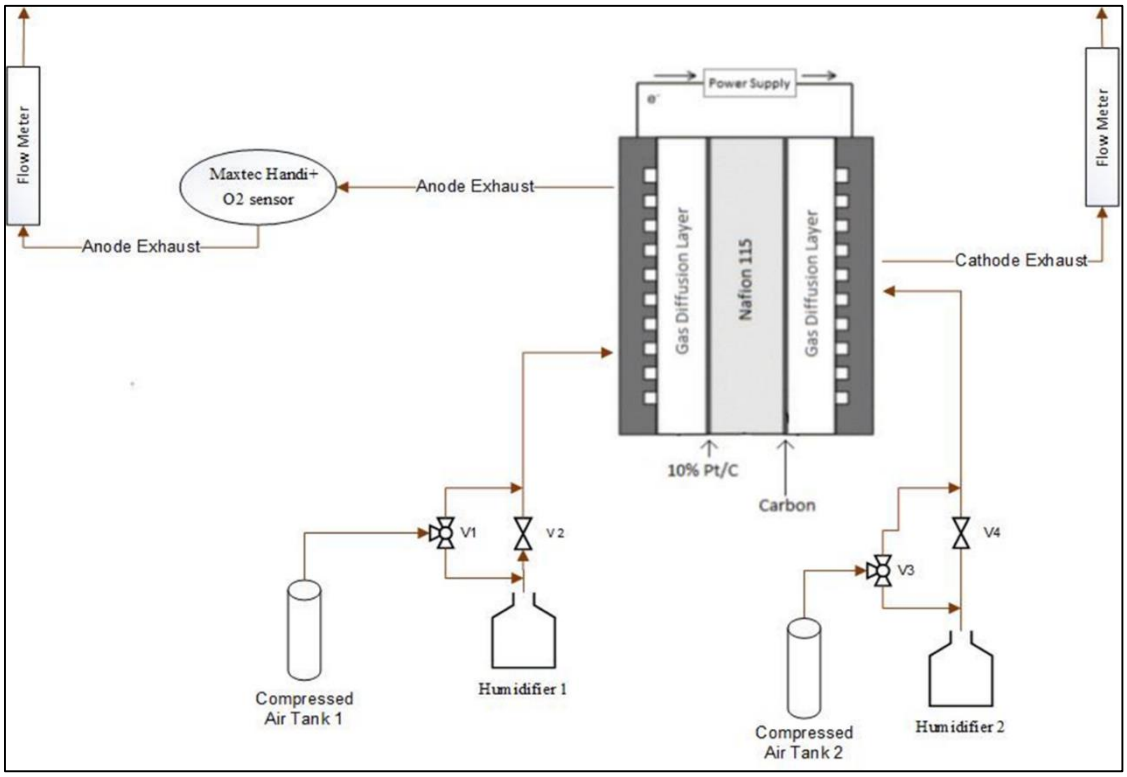

Figure 3.2 A Example Schematic of Experimental Procedure

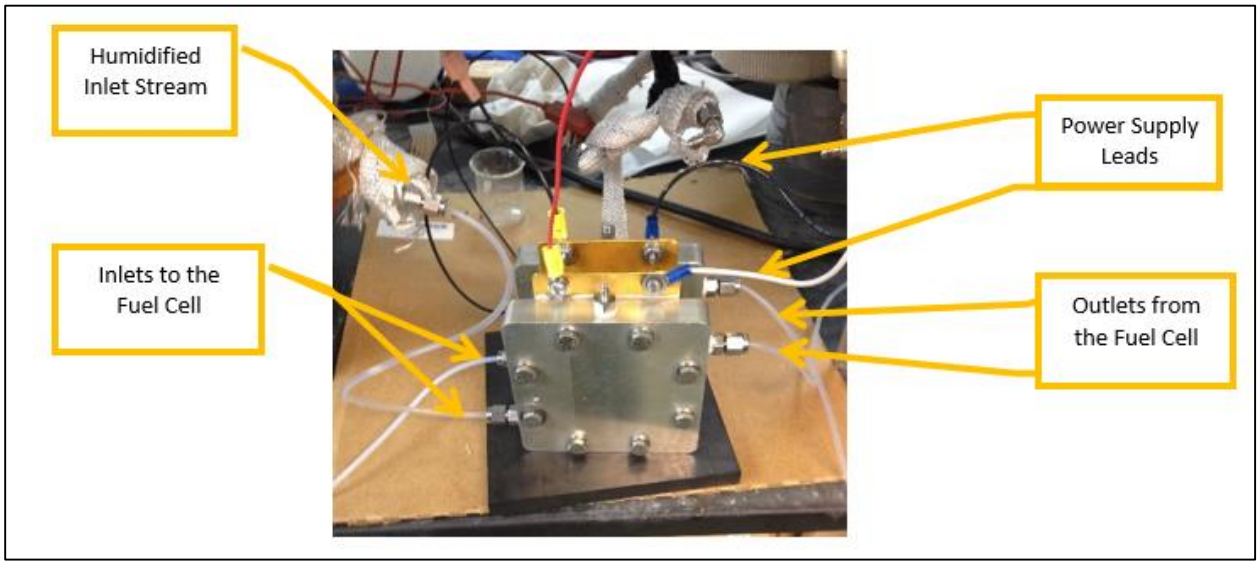

Figure 3.2 B Diagram for the fuel cell where the cathode is receiving the humidified inlet while the anode is receiving a dry inlet. In addition, the fuel cell is connected to the power supply and the Fuel Cell Test System

The MEA was housed in the fuel cell assembly designed for a 5cm^2 MEA as seen in the Figure 3.2B and a sample process flow diagram has been provided in Figure 3.2A. Temperature controlled humidifiers accompanied the test station to provide desired humidified inlets to the fuel cell. In addition, both the anode and cathode were connected to the waste stream to ensure no release of gases to the environment. Swagelok connections were used to ensure no leaks occurred during the experimental runs. The testing station used to conduct the experimental runs was located in the Fuel Cell Center at Worcester Polytechnic Institute as seen in Figure 3.2C.

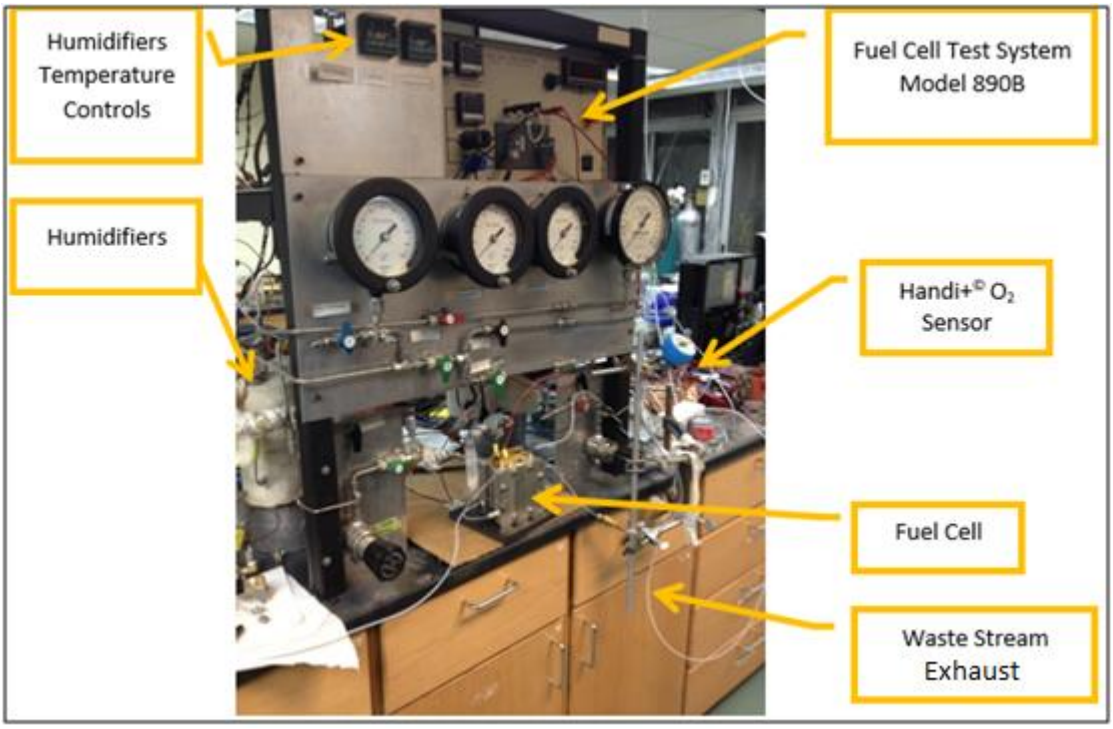

Figure 3.2 C Overall Diagram of the Fuel Cell Test bed located in the Fuel Cell Center at Worcester Polytechnic Institute

Additionally, the test station contained the Fuel Cell Test System Series 89B, alongside a computer interface which plotted the data recorded. This system, was also used to apply small amounts of current (mA) during the activation of the each MEA. The Handi+, a portable battery-powered oxygen sensor manufactured by Maxtec, was used to measure the O_2 concentration in

the product stream with an accuracy of 0.1%. The sensor was calibrated before each MEA that was tested using the oxygen or air tank in Goddard Hall's Fuel Cell Center. The test bed shown in Figure 3.2C contains other pieces of equipment such as valves, piping and pressure gauges which were not necessarily a part of these experimental runs.

The HP 6651A power supply, as seen in Figure 3.2D, was used to apply voltage across the fuel cell during the experimental runs.

Figure 3.2 D HP power supply used for the experimental runs

3.3 Materials

The experimental procedures in this study were carried out using various membrane electrode assemblies (MEAs). Each MEA consisted of a Nafion® 115 membrane, a catalyst layer on each side of the membrane, and a gas diffusion layer on each side of the membrane. All of the MEAs tested had an active transport area of 5 cm^2. Two types of MEAs were used for oxygen transport studies, one with Printex L6 cathode loading and 1 mg Pt/C, the other with 1 mg Pt/C loading on both the cathode and the anode. An MEA for electrolysis was also used in studies, with 1 mg Pt/C loaded at the cathode and 3 mg PtIrB loaded at the anode. A complete summary of the MEAs testing in this study can be seen in Table 3.3A.

Table 3.3 A Summary of Tested MEAs

MEA Name	Membrane	Cathode Catalyst	Anode Catalyst	Product #	Supplier
P1	Nafion® 212	0.5 mg/cm^2 Pt on carbon	0.5 mg/cm^2 Pt on carbon	5L HP-A MEA 5cm^2	FuelCellStore
P2	Nafion® 212	0.5 mg/cm^2 Pt on carbon	0.5 mg/cm^2 Pt on carbon	5L HP-A MEA 5cm^2	FuelCellStore
P3	Nafion® 115	0.1 mg/cm^2 Pt on carbon	0.1 mg/cm^2 Pt on carbon	Custom 5cm^2 MEA	FuelCellsEtc
C1	Nafion® 115	1 mg/cm^2 Printex L6	0.1 mg/cm^2 Pt on carbon	Custom 5cm^2 MEA	FuelCellsEtc
C2	Nafion® 115	1 mg/cm^2 Printex L6	0.1 mg/cm^2 Pt on carbon	Custom 5cm^2 MEA	FuelCellsEtc
I1	Nafion® 115	0.1 mg/cm^2 Pt on carbon	3 mg/cm^2 PtIrB	Custom 5cm^2 MEA	FuelCellsEtc
I2	Nafion® 115	0.1 mg/cm^2 Pt on carbon	3 mg/cm^2 PtIrB	Custom 5cm^2 MEA	FuelCellsEtc

In order to study the transport of hydrogen peroxide across the membrane, a 35% solution of hydrogen peroxide was also obtained from Alfa Aesar. This was used to saturate inlet streams with hydrogen peroxide in an effort to facilitate hydrogen peroxide transport through the membrane.

Various additional materials were used in these experimental procedures. Rotameters were purchased from Cole Parmer and had a flow range from 0 to 3 L/min. Compressed gas tanks containing air, oxygen, hydrogen, and helium were used as the feed to the system. All tubing and fittings were purchased through Swagelok.

3.4 Experimental

The first series of MEAs tested were the standard platinum supported on carbon. To activate these, humidified hydrogen was fed to the anode and humidified air to the cathode for a period of 1 – 3 hours. Following this, a current of 0.5 – 0.6 A was applied for 4 – 5 hours. The final step in the activation was to apply varying currents between 0.4 A and 0.8 A for 15 – 20

minutes each, a total of four times. For the first MEA an ATR-IR spectrum was also taken in-between each step of the activation. At the end of activation a polarization curve was taken by scanning the current from 0 to 3 A in 0.05 A increments, holding each current for 60 seconds.

For MEA P1, the first set of experiments involved feeding humidified air to both sides of the cell and applying a potential of 1.4 V for 20 minutes, then 1.5 V for 30 minutes. The next set of experiments was to feed humidified He to both sides of the cell and apply 1.5 V for an hour, then 1.6 V for 45 minutes. The final experiment was to feed heated humidified He to both sides of the cell, this was accomplished by heating the humidifiers from 11^{o} C to 27^{o} C before beginning the experimental run. Once the humidifiers were at 27^{o} C a potential of 1.6 V was applied for 5 minutes, immediately followed by a potential of 1.8 V for 5 minutes, immediately followed by a potential of 2.0 V for 1 hour. After the first 40 minutes of the experiment the humidifiers were heated to 50^{o} C. At the conclusion of these tests a polarization curve was taken, as described above at the end of the activation, and compared to the first polarization curve to determine the condition of the MEA.

For MEA P2, the first set of experiments involved feeding humidified He to the cathode and dry He to the anode while applying potentials between 1.4 V and 2.0 V for 5 minute intervals. The next set of experiments was to feed humidified air to the cathode and dry air to the anode while applying various potentials between 1.3 V and 2.0 V for 5 minutes apiece. The final set of experiments was to feed dry air to the anode and dry O_2 to the cathode while applying potentials between 0.8 V and 2.0 V for periods of time shorter than 10 minutes. At the conclusion of these

tests a polarization curve was taken, as described above at the end of the activation, and compared to the first polarization curve to determine the condition of the MEA.

For MEA P3, only two experiments were run. First He with H_2O and H_2O_2 vapor was fed to the cathode and humidified air was fed to the anode while applying potentials between 1.0 V and 1.2 V. Then humidified air was fed to the cathode and He with H_2O and H_2O_2 vapor was fed to the anode while applying potentials between 1.0 V and 1.2 V.

The next series of MEAs tested were the Printex L6 (carbon). To activate these, humidified air was fed to both sides overnight, 12 – 20 hours. For MEA C1, the first set of experiments involved applying potentials between 0.4 and 1.0 V while first feeding humidified air to both sides and then dry air to both sides. The next set of experiments was to feed H_2 to the Pt anode and humidified air to the carbon cathode while varying the applied potential. The last set of experiments preformed fed humidified O_2 to the cathode and dry air to the anode while varying the applied potential between 1.0 V and 0.4 V.

For MEA C2, the first set of experiments involved feeding humidified O_2 to the cathode and dry air to the anode while applying varying potentials between 1.3 V and 0.4 V. The next set of experiments involved feeding first dry air then humidified air to the anode and He with H_2O and H_2O_2 vapor to the cathode while varying the applied potential. The third set of experiments was to feed He with H_2O and H_2O_2 vapor to the anode and humidified air to the cathode while varying the potential.

The last series of MEAs tested were standard electrolysis MEAs that had solid Pt/Ir anodes and Pt supported on carbon at the cathode. To activate these MEAs, humidified air was fed to

both sides for an hour. Next humidified air was fed to both sides for 4 – 5 hours and a constant potential of 0.4 V to 0.5 V is applied. The last step was to apply varying potentials between 0.2 V and 0.8 V for 20 minute periods while feeding humidified air to both sides. For MEA I1, the first set of experiments was to feed humidified air to both sides of the cell while varying the applied potential between 1.2 V and 1.8 V and varying the systems temperature between 11^{o} C and 80^{o} C. The next set of experiments was to apply potentials between 1.0 V and 1.2 V while first feeding humidified air to the cathode and He with H_2O and H_2O_2 vapor to the anode; then switching the feeds so that the He with H_2O and H_2O_2 vapor is going to the cathode and the humidified air is going to the anode. The final set of experiments involved feeding humidified O_2 to the cathode and liquid water to the anode while applying 1.4 V to 1.5 V.

The last membrane tested, MEA I2, was tested in four general areas. The first was testing H_2O_2 electrolysis by feeding He with H_2O_2 vapor and H_2O vapor to the anode and feeding humidified air to the cathode while applying potentials between 0.8 V and 1.5 V. The second test was performing liquid water electrolysis rather than vapor electrolysis, and was tested by feeding liquid water to the anode and feeding humidified He to the cathode while applying various potentials between 1.6 V and 2.5 V. The third test was vapor electrolysis, which was tested by feeding both humidified He and air to both sides in turn while applying potentials between 1.2 V and 2.0 V. The final test was an electrolysis driven oxygen pump which was tested by feeding each in turn: dry O_2, humidified O_2, humidified air, and humidified He to the cathode and feeding each in turn: humidified He, humidified air, and liquid water to the anode while applying potentials between 1.2 V and 2.0 V. For the full tabularized list of tests and results on all MEAs, please refer to Appendix A.

4. Results & Discussion

4.1 Liquid Electrolysis

This set of experiments attempted to examine water electrolysis on a proton exchange membrane as a method of transporting oxygen across the membrane as shown in Figure 3.1A. All of the water electrolysis runs were performed with an MEA loaded with Pt/C at the cathode and unsupported PtIrB at the anode. As discussed previously, this process involves the oxidation of water to produce oxygen and hydrogen. Initially, tests were performed in an attempt to perform electrolysis in the MEA. As seen in Table 4.1A, the largest measurable current during these trials was 108 mA. These results were gathered feeding liquid water to the anode of the cell at 10 mL/min. While the oxygen produced was not measured, the presence of gas in the liquid outlet stream and a current signifies that electrolysis is occurring at the membrane. Electrolysis is observed at voltages higher than 1.23 V, which is the theoretical voltage for water electrolysis. As seen in the results, the current density of the cell increases as voltage increases, and a maximum current density is not observed.

Table 4.1 A MEA I2 Liquid Electrolysis Results

Applied Voltage	Current	Humidifier Temperature	Cell Temperature
1.6 V	40 mA	60 C	60 C
1.8 V	67 mA	60 C	60 C
2.0 V	81 mA	60 C	60 C
2.2 V	94 mA	60 C	60 C
2.5 V	108 mA	60 C	60 C

The measured current density for water electrolysis in this study is, however, inexplicably much lower than published values for proton exchange membrane electrolysis (Eladeb et al., 2012; Greenway et al., 2009). A potential cause for this problem is the formation of vapor bubbles on the membrane at the site of water electrolysis. The formation of vapor bubbles in the liquid feed to the cell can seriously hinder the mass transfer and hence the performance of the electrolysis cell. While flowing bubbles can potentially provide transport of liquid water to the membrane, too many bubbles can limit the contact area between the liquid water and the surface of the membrane (Spurgeon & Lewis, 2011). This in turn reduces the amount of electrolysis that occurs. It's very likely that a limiting density can be reached, with the amount of bubbles forming on the membrane limiting any increase in electrolysis, although such a limit was not reached. The flow rate of liquid water may also have an effect on the formation of bubble at the site of electrolysis. Due to the lack of a settable pump, this effect was unable to be measured. Many studies opt for low liquid water flow rates when performing proton exchange membrane electrolysis, although a higher flow rate may be more beneficial due to the likelihood of the flow either pushing the forming vapor to the membrane or flushing it out of the system. It has been shown that a higher stoichiometric ratio of water, associated with a higher flow rate, decreases the current density in an electrolysis membrane (Greenway et al., 2009). It follows that proper operation requires the correct balance between these two parameters. A more in-depth and precise testing procedure would most likely provide a more favorable result.

4.2 Vapor Electrolysis

Vapor electrolysis was also examined in this study using a similar membrane, a Pt/C catalyst at the cathode and unsupported PtIrB catalyst at the anode. The mechanism is exactly

the same as liquid electrolysis, with the exception that water vapor is used as the feed to the system rather than liquid. More trials were attempted to create an oxygen pump using the same membrane. The process would include oxygen reduction at the cathode and water electrolysis at the anode to pass oxygen from the cathode to the anode as seen in Figure 3.1A. In these trials, the current density and the change in oxygen composition were measured to assess the performance of the cell. As seen in the results, these trials provided less than desirable results. At most, the oxygen content of the outlet stream rose 0.3%. A summary table of the complete results of these runs can be found in Appendix A.

Table 4.2 A Vapor Electrolysis Results at Ambient Temperature

Cathode Feed	Anode Feed	Applied Voltage	Observed Current	Change in Oxygen Concentration
Humidified Air at 60 mL/min	Humidified Air at 40 mL/min	1.3 V	26 mA	0.05 %
		1.4 V	40 mA	0.1 %
		1.5 V	47 mA	0.1 %
		1.6 V	53 mA	0.1 %
		1.7 V	60 mA	0.1 %
		1.8 V	67 mA	0.1 %

Table 4.2 B Vapor Electrolysis Results at Elevated Temperature

Cathode Feed	Anode Feed	Applied Voltage	Observed Current	Change in Oxygen Concentration	Humidifier Temperature
Humidified Air at 235 mL/min	Humidified Air at 235 mL/min	1.5 V	94 mA	0.2 %	61 C
		1.5 V	94 mA	0.3 %	65 C
		1.5 V	108 mA	0.1 %	71 C
		1.5 V	163 mA	0.2 %	75 C
		1.5 V	163 mA	0.2 %	80 C

As seen in the results, vapor electrolysis yields similar current densities to that of liquid electrolysis. While vapor electrolysis avoid the problem of bubble formation which was discussed earlier, there are a number of issues with vapor electrolysis. The majority of these problems stem from the mass transport limitations that occur at higher current densities with water vapor (Spurgeon & Lewis, 2011; Greenway et al., 2009; Fox & Colón-Mercado, 2011). A mass flux limit is reached at relatively low values of electrolysis, as water molecules are unable diffuse any faster through the membrane.

This mass flux limit could potentially be caused by two things. The first possible issue with the system is the formation of water in the MEA. It is known that liquid water can be detrimental to the operation of a PEM fuel cell, as the excess presence of water can smother the gas electrodes and ultimately flood it (Pasaogullari & Wang, 2004). This can also be a serious issue at the gas diffusion layer as well (Pasaogullari & Wang, 2004; Litster et al., 2006). When considering

these studies along with the conceptual model of the electrolysis aided oxygen pump, this could be an issue for the oxygen reduction reaction. There is the possibility that too much water could completely flood the gas diffusion layer. If too much water is created at the cathode and the gas diffusion layer is also flooded, oxygen from the cathode inlet stream is prevented from passing through to the catalyst. This could potentially be a cause for a mass flow limitation in the system. While the presence of liquid water in the membrane is beneficial to the system, the level at which it would have to be controlled may be an issue that prevents the design of an efficient system based on an electrolysis aided pump.

Oxygen transport concerns through the gas diffusion layer is a topic of concern as well. It has been shown that the presence of nitrogen in the cathode feed stream significantly reduces the transport of oxygen across the gas diffusion layer (Benzinger et al., 2011). The presence of the nitrogen takes up space in the gas diffusion layer and inhibits oxygen transport. This issue is not unique to this design, as it is also an issue for air-fed PEM fuel cells. Normally operating fuel cells do not seem to have a serious issue with this problem, so it is possible that this should be of no concern in this case. It is more likely that this oxygen transport issue, when combined with the liquid water problem discussed earlier, is a possible hindrance to the operation of the electrolysis aided pump.

Relative humidity is another issue with vapor electrolysis, as the feed streams must be at a relative humidity of 95% or higher, otherwise the electrolysis activity is greatly diminished (Spurgeon & Lewis, 2011). It is assumed here that the relative humidity of the streams in this experiment were of adequate values, although the humidity was never measured. This signifies

that the mass flux limitation is the limiting factor to these trials. Published results show that the voltage at which this limit is reached lies between 1.6 and 2.0 V, at which the current density at room temperature is varying between 40 mA/cm^2 and 90 mA/cm^2 (Spurgeon & Lewis, 2011; Greenway et al., 2009). Using these numbers, the amount of oxygen that could be produced through vapor electrolysis is roughly 1.6 mL/min. The efforts to scale this up to a practical design would not be worthwhile, as the system would require too large of a housing, making it impractical for the intended use as put forth by this study. Although vapor electrolysis can be used to produce oxygen, its mass flow limitations at higher current densities and its requirement for high relative humidity prove it to be impractical.

4.3 Two Electron Oxygen Reduction

This group of experiments examined the two electron oxygen reduction aided O_2 pump (as seen schematically in Figure 3.1B). The first set of experiments were on the carbon (Printex L6) catalyzed MEAs. MEA C1 was tested by applying varying potentials between 0.4 V and 1.0 V while feeding different gases to the cell. We tested dry air to both sides, humidified air to both sides, and humidified O_2 to the cathode with dry air to the anode. No current or change in percent O_2 where observed for all trials. This lack of generated current indicates that the desired 2 e^- ORR and O_2 transfer was not achieved, as further supported by the static O_2 levels observed during the tests. After these tests, MEA C1 was run in fuel cell mode by feeding humidified O_2 to the cathode and dry H_2 to the anode resulting in an OCV of 0.20 V. This OCV indicates a very low level of electrochemical active and as such, prompted the end of testing on MEA C1.

MEA C2 was tested by applying potentials between 0.4 V to 1.3 V while feeding humidified O_2 to the cathode with dry air to the anode. No current or change in O_2 levels were observed

below 1.2 V. However, small currents of 12 mA and 26 mA were observed at 1.2 V and 1.3 V respectively, with no discernable change in percent O_2 in the anode exhaust. The complete lack of activity below 1.2 V indicates the desired O_2 transfer was not achieved. Additionally the small currents achieved at and above 1.2 V show that MEA C2 is electrochemically active and capable of H_2O_2 electrolysis. Next MEA C2 was tested by applying potentials between 1.0 V and 2.5 V while feeding humidified air to the anode with He bubbled through 35% H_2O_2 fed to the cathode. Below 1.2 V there was no observable current or change in O_2 levels. At higher potentials an increase in current and decrease in O_2 at the anode exhaust was observed up to 135 mA and –4.2% O_2 at 2.5 V, once again indicating that MEA C2 is electrochemically active and capable of H_2O_2 electrolysis. The final testing for MEA C2 involved applying potentials between 1.0 V and 1.2 V while feeding humidified air to the cathode with He bubbled through 35% H_2O_2 to the anode. For these final trials no change in current or O_2 levels where observed.

The next MEA tested was a standard fuel cell MEA with Pt supported on carbon as the catalyst for both sides. First varying potentials between 1.0 V and 1.2 V were applied while humidified air was fed to the cathode and He bubbled through H_2O_2 was fed to the anode. No change in O_2 levels or current was observed. Next He bubbled through H_2O_2 was fed to the cathode and humidified air was fed to the anode while potentials between 1.0 V and 1.2 V were applied. Each of these trials generated a small current and a small decrease in O_2 levels, as seen in Table 4.3A. This small decrease in O_2 levels at the anode coupled with potentials under 1.2 V suggest that we are electrolyzing the supplied H_2O_2 at the cathode and transporting H^+ across the membrane to form H_2 at the anode.

Table 4.3 A Test result for MEA P3 with He bubbled through H2O2 fed to the cathode and humidified air fed to the anode

Applied Potential	% O_2 Start	% O_2 End	Current
1.0 V	20.6 %	20.5 %	12 mA
1.1 V	20.6 %	20.4 / 20.5 %	26 mA
1.2 V	20.6 %	20.3 / 20.4 %	40 mA

The final set of MEAs tested were standard water electrolysis MEAs with an Ir/Pt anode catalyst and a Pt supported on carbon cathode catalyst. On MEA I1 two experiments were run; first He bubbled through 35% H_2O_2 was fed to the anode with humidified air fed to the cathode while applying potentials between 1.0 V and 1.2 V. Then He bubbled through 35% H_2O_2 was fed to the cathode with humidified air fed to the anode while potentials between 1.0 V and 1.2 V were applied. In both experiments no current or change in O_2 was observed. However, when the first above experiment was repeated on MEA I2, with flow rates of 250 ml/minute, a small current and a small change in O_2 were observed, as seen in Table 4.3B.

In both MEA I2 and MEA P3 H_2O_2 vapor was fed to the anode and small currents were obtained. This indicates that the Ir/Pt and Pt supported on carbon catalysts are capable of H_2O_2 electrolysis to O_2 as is necessary for our conceptual model to work.

Table 4.3 B Test results for MEA I2 with humidified air feed to the cathode and He bubbled through H2O2 feed to the anode

Applied Potential	Change in O_2	Observed Current	Theoretical change in O_2 based on current
1.0 V	0.10%	40 mA	0.11%
0.8 V	0%	6 mA	0.02%
0.9 V	0%	20 mA	0.06%
1.5 V	0.30%	149 mA	0.41%
1.2 V	0.15%	81 mA	0.23%
1.1 V	0.10%	53 mA	0.15%

4.4 Carbon Degradation

Towards the end of testing on MEA P1, MEA P2, MEA P3, MEA I1, and MEA I2 there was a noticeable drop in performance on repeated tests. This is most likely due to degradation of the carbon supporting the Pt catalyst at the cathode. Zhang et al. (2009) summarizes this type of carbon degradation by reviewing a number of studies on the degradation of Vulcan XC 72R carbon supports in Pt supported on carbon fuel cells. They discuss how potentials in excess of 1.0 V degrade the carbon supports through CO_2 production as seen in Table 4.4A. Additionally lack of fuel can speed up the carbon degradation as the applied potential has no pathway other than the carbon degradation to proceed by. As many of our experiments were unsuccessful in achieving the desired reaction, the cell was essentially in a state of fuel starvation. Additionally for the H_2O_2 electrolysis seen on MEA I2 in Table 4.3B (above), the theoretical H_2O_2 production for potentials at or above 1.0 V is higher than the observed. This is consistent with the description of carbon degradation that we are given by Zhang et al. (2009).

Table 4.4 A Surface Carbon Degradation

$C_s \rightarrow C_s^+ + e^-$
$C_s^+ + 1/2\ H_2O \longrightarrow C_sO + H^+$
$C_sO + H_2O \longrightarrow CO_2(g) + 2H^+ + 2e^-$

** C_s denotes a surface species*

At the end of testing MEA C1 and MEA C2, a significant drop in electrochemical activity is seen, as discussed earlier in section 4.3. This is most likely due to degradation of the Printex L6 carbon catalyst from prolonged high voltage and fuel starved testing as discussed with the carbon supports above.

5. Conclusion and Recommendations

5.1 Conclusion

In this study, oxygen transport through a proton exchange membrane fuel cell was examined in an effort to develop an efficient and effective oxygen pump. The examined MEAs were loaded with catalysts such as Pt/C, Printex L6, and PtIrB in varying combinations. Each MEA was run under a varying number of conditions, including feed stream composition, applied voltage, and temperature. The change in oxygen concentration of the outlet streams and the generated current were observed and recorded.

As seen in the results for the vapor electrolysis trials, any significant oxygen generation at the anode of the cell was unattainable in these experiments. The inability to sustain a large current during vapor electrolysis inhibits the ability of the cell to transport oxygen across the membrane. While increasing cell size, stacking multiple membranes, and increasing the cell operating temperature could increase the oxygen yield, these changes to the cell would not make it any more viable. The membrane area and stacking number of membranes required to achieve significant oxygen transport would be too large for the design to be a compact and convenient size. Increasing the temperature of the cell would inhibit the use of the cell as a safe personal oxygen generator.

In terms of the two electron reduction transport of oxygen, neither the Pt/C catalyst nor the Printex L6 catalyst was effective in promoting two electron reduction at the cathode. Oxygen transport was comparable to that of the electrolysis aided pump, and as such neither system would be suitable for this application. Based on these results, an attempted scale up of these systems to achieve an effective full-size model would ultimately prove futile.

While the vapor electrolysis aided pump is most likely to be ineffective as a method of oxygen transport, the two electron oxygen reduction method may show some promise in future testing. The primary issue with the Pt/C and Printex L6 catalyst is that they failed to foster the formation of hydrogen peroxide at the cathode of the cell. Further research has revealed a number of catalysts that are more selective for and much more effective for the reduction of oxygen to hydrogen peroxide. Any further research on this project must begin with the examination of different catalysts for the oxygen reduction reaction. Subsequent design of the device can most likely be successfully continued from that point.

5.2 Recommendations

The encouraging preliminary results of this project should be followed up with additional research as suggested to determine the feasibility of oxygen pumping across ion exchange membrane for the development of an oxygen generator.

5.2.1 Use of Alternative Catalysts

When considering the use of catalysts to assist in this reaction, the following catalysts come to mind: Pt/C, Pt/Ni and Pt/Ag. This project was only able to conduct preliminary testing on carbon catalysts. Furthermore, the team has found related research suggesting a variety of catalysts to test at the cathode side.

Research studies have shown promising results regarding the electrochemical reduction of oxygen to hydrogen peroxide will be discussed next. For the PEM oxygen pump design, the cathode side reaction involves the reduction of oxygen to (or production of) hydrogen peroxide. It is evident that the reaction will require an active, selective and stable catalyst to catalyze the reaction. Siahrostmi's study shows Pt-Hg (mercury) to be promising through initial calculations

(Siahrostami et al., 2013). In addition, electrochemical measurements suggest Pt-Hg nanoparticles shows more than an order of magnitude of improvement in mass activity as seen in the Figure 6.1A below (Siahrostami et al., 2013). It can be seen from Figure 6.1A that the activity of only platinum is very inefficient. Therefore, Siahrostami results and this project study on carbon should be taken in consideration for further experiments.

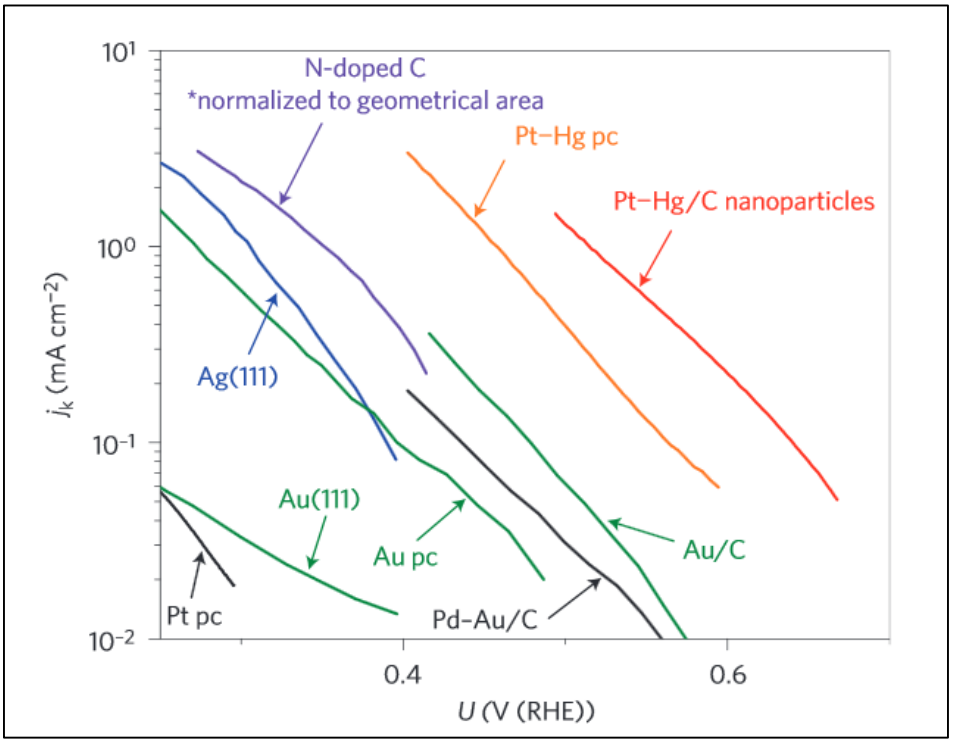

Figure 6.1 A Overview of different electro catalysts for H2O2 production (Siahrostami et al., 2013)

Another study focusing on the anode side reactions suggests a possible catalyst layer that could be studied to help control the production of H_2O_2. This study shows a decrease in cathode open circuit voltage, OCV, correlates to the amount of H_2O_2 generated within the membrane (Jung, 2007). The study confirms that a PEMFC with a Pt/ RuC layer at the anode, experiences a high OCV thus suggesting a lower concentration of H_2O_2. Though Jung's findings show do not

directly relate to this section, it important to understand potential relationships between testing parameters.

5.2.2 Fabricating Membranes

As the alternative catalysts suitable for future tests are to be explored, a recommendation is made to fabricate MEAs with these catalysts accessible commercially. When considering the further testing of MEAs fabricating, MEAs in the lab will help ensure proper preparations of membranes since the preparation procedure will be consistent for each MEA created. A sample procedure has been provided in Appendix C. Further research describes some common procedures used to load catalysts onto membranes such as the use of spray gun to apply the platinum onto the membrane under an infrared lamp (Leimin et al., 2009). Additionally, a sputter technique has been proven to be a useful method to apply minimal amounts (such as nanoparticles) of platinum on PEMs especially onto Nafion® (Wee et al., 2010). This method could potentially be adapted for to construct the Pt/Hg-C nanoparticles membrane previously discussed. The primary benefit for fabricating membranes by hand is the freedom to test various catalysts.

5.2.3 Stacking

If future results are more promising than those in this study, scale up would require testing MEAs in series as seen in the Figure 6.3A, which will be important for the scale up requirement

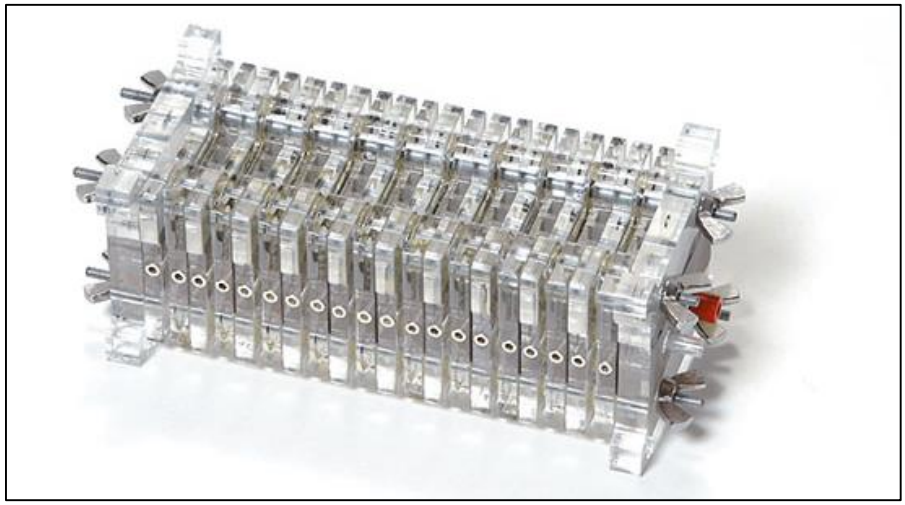

Figure 6.3 A Sample Fuel Cell Stack (Fuel Cell Store, 2013)

for the oxygen generation device. In order to achieve the desired volumetric flow of enriched O_2 multiple MEAs together otherwise, i.e., a fuel cell stack, will need to thoroughly investigate. The project team suggests focusing on the total current density achieved, amount of O_2 produced and amount of time need to produce O_2.

5.2.4 Anion Exchange Membranes

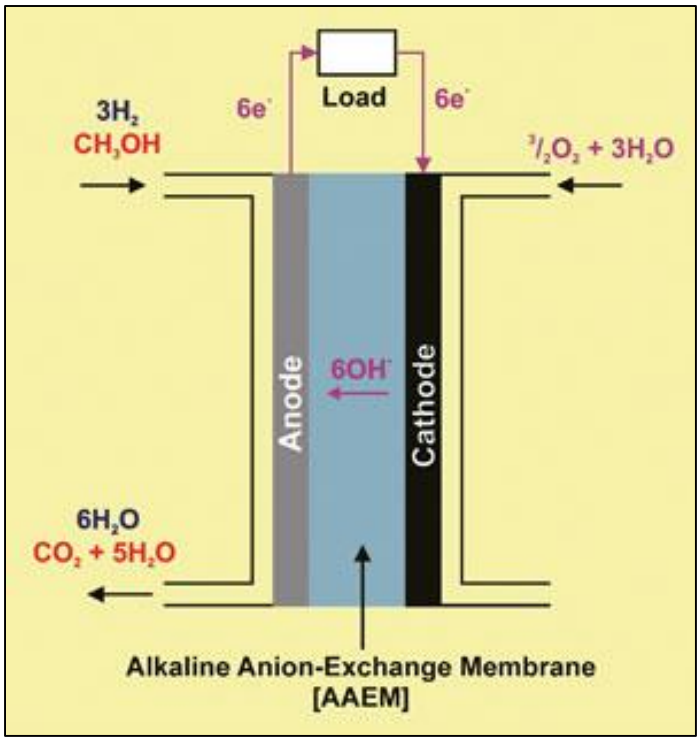

Figure 6.4 A Sample Anion Exchange Membrane for metal cation-free alkaline fuel cell

PEMs are not the only the type membranes viable for conducting such experiments. Anion exchange membranes (AEM) behave similar to PEMs, however, instead of the proton (+) a negative charge (-) passes across the membrane. The restriction on time did not allow for the testing of AEM membranes, however, background section 2.4 on AEM will be useful for further studies. Utilizing MEAs based on AEMs, which might prove to be more effective than based on PEMs.

5.2.5 Mathematical Analysis

Mathematical analysis can be insightful. A useful recommendation for future researchers is to develop a PEM fuel cell (PEMFC) model for oxygen pumping using COMSOL Multiphysics. COMSOL Multiphysics is a software package that allows for an interactive environment for modeling and simulating scientific and engineering problems. The model can be used a tool to

better understand the physics of PEMFC based oxygen pump. The following figure is an example of the PEMFC modeled in COMSOL.

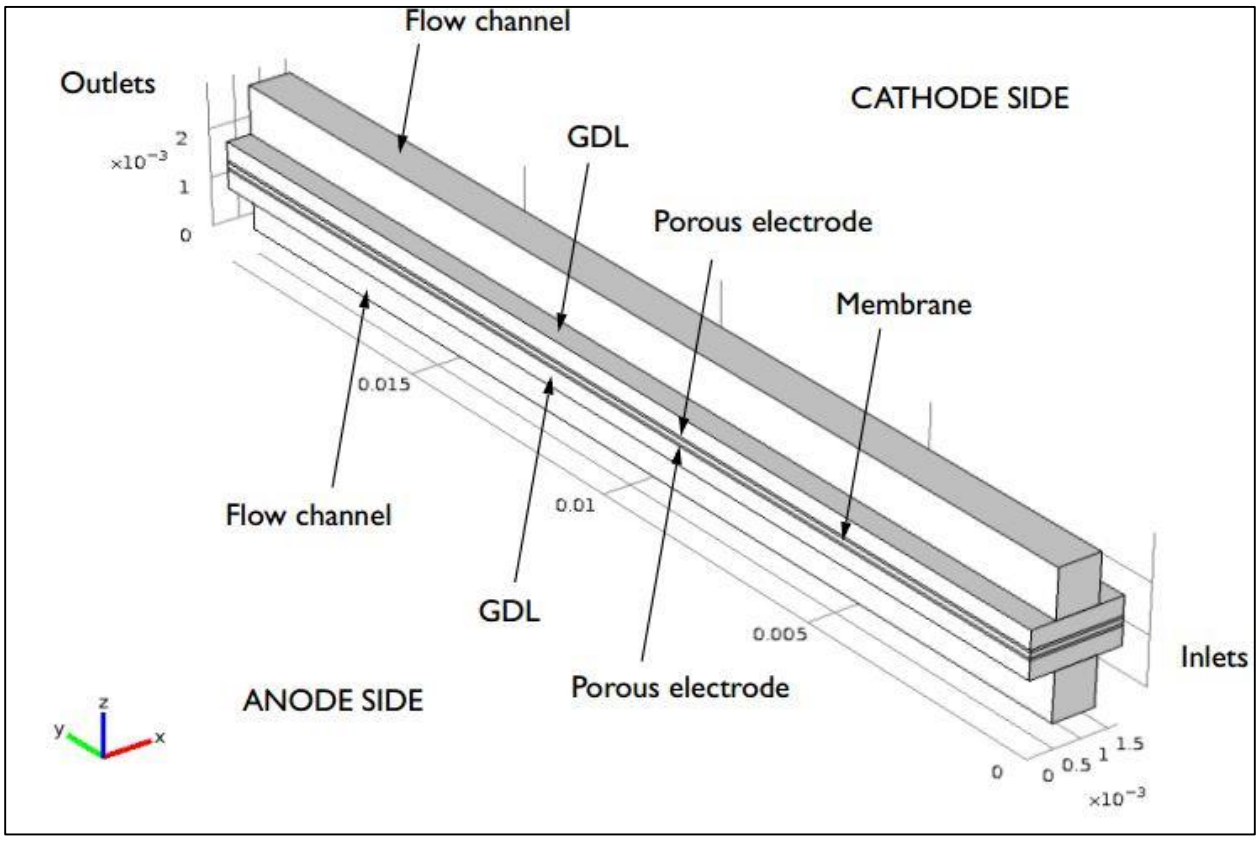

Figure 6.5 A Geometry of a proton exchange membrane (PEM) modeled in COMSOL Multiphysics. (COMSOL Multiphysics, 2014)

The makers of COMSOL have provided the following example of an analysis when modeling a PEMFC: ***Ohmic Losses and Temperature Distribution in a Passive PEM Fuel Cell***

A sample graph from the results of the case study above can be found in Appendix D. The main recommendation for future researchers is to develop and use a COMSOL model as a tool to gain a better understanding on the concept of the oxygen pump and testing parameters. In addition, COMSOL can help provide a theoretical approach and provide a basis on what to expect before conducting experimental in the laboratory.

Works Cited

Arges, C.G., Ramani, V, and Pintauro, P.N. (2010). Anion Exchange Membrane Fuel Cells. *Electrochem. Soc. Interface.* 19. 31-35.

Assumpção, M. H. M. T., De Souza, R. F. B., Rascio, D. C., Silva, J. C. M., Calegaro, M. L., Gaubeur, I., Paixão, T. R. L. C., & Hammer, P. (2012). A comparative study of the electrogeneration of hydrogen peroxide using vulcan and printex carbon supports. *Carbon*, *49*(8), 2842–2851.

Benziger, J., Kimball, E., Mejia-Ariza, R., & Kevrekidis, I. (2011). Oxygen mass transport limitations at the cathode of polymer electrolyte membrane fuel cells. *AIChE Journal*, *57*(9), 2505-2517.

Boehm, H. P., Mair, G., Stoehr, T., deRincon, A. R., & Tereczki, B. (1984). Carbon as a catalyst in oxidation reactions and hydrogen halide elimination reactions. *Fuel*, *63*(8), 1061-1063.

Brillas, E., A. Maestro, M. Moratalla, and J. Casado. "Electrochemical extraction of oxygen from air via hydroperoxide ion." Journal of applied electrochemistry 27, no. 1 (1997): 83-92.

Choi, P., Jalani, N. H., Thampan, T. M., and Datta, R., "Consideration of Thermodynamic, Transport, and Mechanical Properties in the Design of Polymer Electrolyte Membranes for Higher Temperature Fuel Cell Operation," J. Polymer Sci. B: Polymer Phys., 44, 2183 - 2200 (2006).

Coms, F. D. (2008). The chemistry of fuel cell membrane chemical degradation.*ECS Transactions*, *16*(2), 235-255.

COMSOL Blog. (n.d.). *PEM Fuel Cell Modeling Examples*. Retrieved April 23, 2014, from http://www.comsol.com/blogs/pem-fuel-cell-modeling-examples/

Eladeb, Boulbaba, Caroline Bonnet, Eric Favre, and François Lapicque. "Electrochemical extraction of oxygen using PEM electrolysis technology." Platinized titanium dioxide electrodes for methanol oxidation and photo-oxidation: 211 (2012).

Fox, E. B., & Colón-Mercado, H. R. (2011). Mass transport limitations in proton exchange membrane fuel cells and electrolyzers. *Mass Transfer—Advanced Aspects*.

Fuel Cell Store. (n.d.). *FuelCellStore.com*. Retrieved April 23, 2014, from http://www.fuelcellstore.com/en/pc/viewcategories.asp?idCategory=8

Fujita, Y., Nakamura, H., & Muto, T. (1985). An electrochemical oxygen separator using an ion-exchange membrane as the electrolyte. *Journal of Applied Electrochemistry*, *16*(6), 935-940. doi: 10.1007/BF01006541

Greenway, S. D., Fox, E. B., & Ekechukwu, A. A. (2009). Proton exchange membrane (PEM) electrolyzer operation under anode liquid and cathode vapor feed configurations. *International journal of hydrogen energy*, *34*(16), 6603-6608.

Grew, K. N., Chu, D., and Chiu, W. K. S., "Ionic Equilibrium and Transport in the Alkaline Anion Exchange Membrane," J. Electrochem. Soc., 157, B1024-B1032 (2010).

Gauthier, W. D., Hendricks, M. J., & Babcock, R. L. U.S. Patent and Trademark Office, (1980). *Oxygen enrichimient system for medical use* (US4222750 A).

Hydrogen peroxide. In (1974). D. Considine (Ed.), *Chemical and Process Technology Encyclopedia*. New York: McGraw-Hill Book Company.

Jung, U. H., Jeong, S. U., Chun, K., Park, K. T., Lee, H. M., Choi, D. W., & Kim, S. H. (2007). Reduction of hydrogen peroxide production at anode of proton exchange membrane fuel cell under open-circuit conditions using ruthenium–carbon catalyst. *Journal of power sources*, *170*(2), 281-285.

Langer, S. H., & Haldeman, R. G. (1964). Electrolytic Separation and Purification of Oxygen from a Gas Mixture. *The Journal of Physical Chemistry*, *68*(4), 962-963.

Leimin, X., Shijun, L., Lijun, Y., & Zhenxing, L. (2009). Investigation of a Novel Catalyst Coated Membrane Method to Prepare Low-Platinum-Loading Membrane Electrode Assemblies for PEMFCs. *Fuel Cells*, *9*(2), 101-105.

Litster, S., & McLean, G. (2004). PEM fuel cell electrodes. Journal of Power Sources, 130(1), 61-76.

Litster, S., Sinton, D., & Djilali, N. (2006). Ex situ visualization of liquid water transport in PEM fuel cell gas diffusion layers. *Journal of Power Sources*, *154*(1), 95-105.

Ma, C. A., & Yu, W. G. (1995). An electrochemical device for oxygen production avoiding the generation of hydrogen. *Journal of Applied Electrochemistry*,*26*(8), 881-885. doi: 10.1007/BF00683751

Mauritz, K. A., & Moore, R. B. (2004). State of understanding of Nafion®. *Chemical reviews*, *104*(10), 4535-4586.

Merle, G., Wessling, M., and Nijmeijer, K., "Anion Exchange Membranes for Alkaline Fuel Cells: A Review," J. Memb. Sci., 377, 1-35 (2011).

Panizza, M., & Cerisola, G. (2008). Electrochemical generation of h2o2 in low ionic strength media on gas diffusion cathode fed with air. *Electrochimica Acta*, *54*(2), 876–878. Retrieved from http://www.sciencedirect.com/science/article/pii/S0013468608009390

Pasaogullari, U., & Wang, C. Y. (2004). Liquid water transport in gas diffusion layer of polymer electrolyte fuel cells. *Journal of the Electrochemical Society*, *151*(3), A399-A406.

Siahrostami, S., Verdaguer-Casadevall, A., Karamad, M., Deiana, D., Malacrida, P., Wickman, B., ... & Rossmeisl, J. (2013). Enabling direct H2O2 production through rational electrocatalyst design. Nature materials, 12(12), 1137-1143.

Sigma Aldrich, Nafion® 117. (n.d.). Nafion® 117, thickness 0.007 in.. Retrieved April 30, 2014, from http://www.sigmaaldrich.com/catalog/product/aldrich/274674?lang=en&region=US

Soltani, R. D. C., Rezaee, A., Khataee, A. R., & Godini, H. (2012). Electrochemical generation of hydrogen peroxide using carbon black-, carbon nanotube-, and carbon black/carbon nanotube-coated gas-diffusion cathodes: effect of operational parameters and decolorization study. *Research on Chemical Intermediates*, *39*(9), 4277-4286. doi: 10.1007/s11164-012-0944-8

Song, C., & Zhang, J. (2008). *Electrocatalytic oxygen reduction reaction*. (pp. 89-134). Springer London.

Spurgeon, J. M., & Lewis, N. S. (2011). Proton exchange membrane electrolysis sustained by water vapor. *Energy & Environmental Science*, *4*(8), 2993-2998.

Sudoh, M., Kitaguchi, H., & Koide, K. (1985). Electrochemical production of hydrogen peroxide by reduction of oxygen. *Journal of Chemical Engineering of Japan*, *18*(5), 409-414.

Sulfuric Acid Molecule. (n.d.). Global Warming Art RSS. Retrieved April 30, 2014, from http://www.globalwarmingart.com/wiki/File:Sulfuric_Acid_Molecule_VdW_png

Takenaka, H., Torikai, E., Kawami, Y., & Sakai, T. (1982). Extended Abstracts of the 6th Chlor-alkali Industry Technology Symposium. Electrochem. Soc. Japan, Kyoto. Pg 17.

Tseung, A. C. C., and S. M. Jasem. "An integrated electrochemical-chemical method for the extraction of O2 from air." Journal of Applied Electrochemistry 11, no. 2 (1981): 209-215.

Varcoe, J., Bruen, L., Chan, N., Flack, N., Girard, D., Handsel, J., Kizewski, J., Murphy, S., Poynton, S., Slade, R., Waller, T., and Zeng, R., “Anion-Exchange Polymers and Non-Platinum Catalysts for Alkaline Polymer Electrolyte Membrane Fuel Cell,” Abstract #606, 218th ECS Meeting, Electrochem. Soc. (2010).

Vega, J. A., Chartier, C., & Mustain, W. E., “Effect of Hydroxide and Carbonate Alkaline Media on Anion Exchange Membranes,” Journal of Power Sources, 195(21), 7176-7180 (2010).

Wee, J. H., Lee, K. Y., & Kim, S. H. (2007). Fabrication methods for low-Pt-loading electrocatalysts in proton exchange membrane fuel cell systems. *Journal of Power Sources*, *165*(2), 667-677.

Wilson, M. S. (1993). U.S. Patent No. 5,211,984. Washington, DC: U.S. Patent and Trademark Office.

Winnick, J. (1990). Electrochemical separation of Gases. Advances in Electrochemical Science and Engineering, 1(3), 205-214.

Zhang, S., Yuan, X., Hin, J., Wang, H., Friedrich, A., & Schulze, M. (2009). A review of platinum-based catalyst layer degradation in proton exchange membrane fuel cells. *Journal of Power Sources*, *194*, 588-600.

Zhou, X., Chen, Z., Delgado, F., Brenner, D., & Srivastava, R. (2007). Atomistic simulation of conduction and diffusion processes in Nafion® polymer electrolyte and experimental validation. Journal of The Electrochemical Society, 154(1), B82-B87.

Appendix A: Results summary table

MEA	*Gas*		*Applied Potential*	*Change in O2*	*Current*	*Humidifier Temp*	*Misc.*
	Cathode	**Anode**					
MEA P1	Hydrogen	Air	Only ran in fuel cell mode.			11 C	
MEA P2	Humidified He	Dry He	1.6 V	0%	12 mA	11 C	
			1.7 V	0.10%	53 mA	11 C	
			1.8 V	0.40%	108 mA	11 C	
			1.9 V	0.70%	176 mA	11 C	
			2.0 V	0.70%	203 mA	11 C	
	Humidified Air	Dry Air	1.6 V	0.70%	203 mA	11 C	
			1.3 V	0.10%	40 mA	11 C	
			1.5 V	0%	53 mA	11 C	
			1.6 V	-0.10%	81 mA	11 C	
			1.7 V	-0.10%	108 mA	11 C	
			1.8 V	-0.10%	122 mA	11 C	
			1.9 V	-0.10%	108 mA	11 C	
			2.0 V	-0.15%	108 mA	11 C	
	Dry Oxygen	Dry Air	1.2 V	0%	10 mA	11 C	
			1.4 V	0%	22 mA	11 C	
			1.6 V	-0.10%	67 mA	11 C	

			1.8 V	-0.10%	94 mA	11 C	
			2.0 V	0%	108 mA	11 C	
			0.8 V	0%	0 mA	11 C	
			1.0 V	0%	0 mA	11 C	
			1.2 V	0%	0 mA	11 C	
			1.4 V	0%	12 mA	11 C	
			1.8 V	0%	10 mA	11 C	
MEA C1	Humidified Air	Humidified Air	0.4 V - 1.0 V	0% for all runs	0 A for all runs	11 C	
	Dry Air	Dry Air	0.4 V - 1.0 V	0% for all runs	0 A for all runs	11 C	
	Humidified O_2	Hydrogen	Run in fuel cell mode for 14 minutes			11 C	
	Humidified O_2	Dry Air	0.4 V - 1.0 V	0% for all runs	0 A for all runs	11 C	

MEA C2	Humidified O_2	Dry Air	0.4 V - 1.0 V	0% for all runs	0 A for all runs	11 C	
			1.1 V	0%	0 mA	11 C	
			1.2 V	0%	12 mA	11 C	
			1.3 V	0%	26 mA	11 C	
	He & H_2O_2 Vapor	Dry Air	1.0 V	0%	0 mA	11 C	
			1.2 V	0%	0 mA	11 C	
			2.0 V	-0.70%	108 mA	11 C	
			2.5 V	-4.20%	135 mA	11 C	
			4.5 V	-3.60%	176 mA	11 C	
	Humidified Air	He & H_2O_2 Vapor	1.0 V - 1.2 V	0% for all runs	0 A for all runs	11 C	
	He & H_2O_2 Vapor	Humidified Air	1.0 V - 1.2 V	0% for all runs	0 A for all runs	11 C	
MEA P3	He & H_2O_2 Vapor	Humidified Air	1.0 V	-0.10%	12 mA	11 C	
			1.1 V	-0.15%	26 mA	11 C	
			1.2 V	-0.25%	40 mA	11 C	
	Humidified Air	He & H_2O_2 Vapor	1.0 V - 1.2 V	0% for all runs	0 A for all runs	11 C	

MEA I1	*Humidified Air*	*Humidified Air*	*1.2 V*	*0%*	*40 mA*	*11 C*	
			1.3 V	0.05%	26 mA	11 C	
			1.4 V	0.10%	40 mA	11 C	
			1.5 V	0.10%	47 mA	11 C	
			1.6 V	0.10%	53 mA	11 C	
			1.7 V	0.10%	60 mA	11 C	
			1.8 V	0.10%	67 mA	11 C	
	Humidified Air	Humidified Air	1.4 V	0%	40 mA	40 C	
			1.6 V	0%	40 mA	40 C	
			1.8 V	0%	53 mA	40 C	
	Humidified Air	He & H_2O_2 Vapor	1.0 V - 1.2 V	0% for all runs	0 A for all runs	11 C	
	He & H_2O_2 Vapor	Humidified Air	1.0 V - 1.2 V	0% for all runs	0 A for all runs	11 C	
	Humidified Air	Humidified Air	1.8 V	0%	12 mA	11 C	
			1.7 V	0%	12 mA	11 C	**Cell Temp**
			1.6 V	0%	0 mA	11 C	
	Humidified O2	Liquid Water	1.5 V	NA	53 mA	11 C	
	FR = 63 ml/min	FR = 10 ml/min	Positive potential at anode				
	Humidified Air	Humidified Air	1.4 V	0.20%	53 mA	80 C	60 C
	FR = 60 ml/min	FR = 40 ml/min	1.5 V	0.20%	40 mA	80 C	60 C
	Positive potential at anode						

MEA I1 (Cont.)	Humidified Air	Humidified Air	1.4 V	-0.15%	12 mA	80 C	60 C
	FR = 60 ml/min	FR = 40 ml/min	Positive potential at cathode				
	Dry Oxygen	Humidified Air	1.4 V	0.10%	12 mA	80 C	60 C
	FR = 40 ml/min	FR = 60 ml/min	Positive potential at cathode				
	Humidified O2	Liquid Water	1.4 V	0%	0 mA	80 C	60 C
	FR = 60 ml/min	FR = 10 ml/min	Positive potential at cathode				

MEA I2	*FR = 250 ml/min*	*FR = 250 ml/min*	*1.3 V*	*0.20%*	*81 mA*	*11 C*	
	Positive potential at anode		1.2 V	0.20%	67 mA	11 C	**ml O2 per Min**
	Humidified Air	He & H_2O_2 Vapor	1.0 V	0.10%	40 mA	11 C	0.27855
	FR = 250 ml/min	FR = 250 ml/min	0.8 V	0%	6 mA	11 C	0.04178
	Positive potential at anode		0.9 V	0%	20 mA	11 C	0.13927
			1.5 V	0.30%	149 mA	11 C	1.037596
			1.2 V	0.15%	81 mA	11 C	0.56406
			1.1 V	0.10%	53 mA	11 C	0.369078
	Humidified Air	Humidified Air	1.5 V	0.20%	84 mA	11 C	
	FR = 235 ml/min	FR = 235 ml/min	1.3 V	0.20%	53 mA	11 C	
	Positive potential at anode		1.2 V	0.15%	47 mA	11 C	
			1.0 V	0.10%	20 mA	11 C	
	Humidified Air	Humidified Air	1.5 V	0.20%	94 mA	61 C	
	FR = 235 ml/min	FR = 235 ml/min	1.5 V	0.30%	94 mA	65 C	
	Positive potential at anode		1.5 V	0.10%	108 mA	71 C	
			1.5 V	0.20%	163 mA	75 C	
			1.5 V	0.20%	163 mA	80 C	

MEA I2 .	*Humidified Air*	*Humidified Air*	*1.5 V*	*0%*	*0 mA*	*11 C*	
	FR = 235 ml/min	FR = 235 ml/min	1.3 V	0%	0 mA	11 C	
	Positive potential at cathode		1.3 V	0%	0 mA	60 C	
	Dry Oxygen	Humidified Air	1.3 V	0%	0 mA	11 C	
	FR = 235 ml/min	FR = 235 ml/min	Positive potential at cathode				
	Dry Oxygen	Liquid Water	1.4 V	0%	0 mA	11 C	Cell Temp unheated
	FR = 235 ml/min	Positive potential at cathode	1.4 V	0%	0 mA	11 C	60 C
	Humidified Air	Humidified He	1.6 V	0%	0 mA	11 C	60 C
	FR = 235 ml/min	FR = 235 ml/min	1.8 V	0%	0 mA	11 C	60 C
	Positive potential at cathode		2.0 V	0%	0 mA	11 C	60 C
	Humidified He	Humidified He	1.3 V	0%	0 mA	60 C	60 C
	FR = 2.4 ml/min	FR = 3.4 ml/min	Positive potential at cathode				
	Humidified He	Humidified He	1.6 V	0.50%	72 mA	60 C	60 C
	FR = 20 ml/min	FR = 17 ml/min	1.7 V	0%	0 mA	60 C	60 C
	Positive potential at anode		1.8 V	0%	0 mA	60 C	60 C

MEA I2			1.8 V	0%	0 mA	60 C	60 C
	Humidified He	Humidified He	1.7 V	0%	0 mA	60 C	60 C
	FR = 35 ml/min	FR = 35 ml/min	1.6 V	0%	0 mA	60 C	60 C
	Positive potential at anode		1.5 V	0%	0 mA	60 C	60 C
	Humidified He	Humidified He	1.6 V	0%	0 mA	60 C	60 C
	FR = 63 ml/min	FR = 76 ml/min	1.8 V	0%	0 mA	60 C	60 C
	Positive potential at anode						
	Humidified He	Humidified He	1.6 V	0%	0 mA	60 C	60 C
	FR = 119 ml/min	FR = 146 ml/min	1.8 V	0%	0 mA	60 C	60 C
	Positive potential at anode						
	Humidified He	Liquid Water	1.6 V	NA	40 mA	60 C	60 C
	FR = 80 ml/min	FR = 10 ml/min	1.8 V	NA	67 mA	60 C	60 C
	Positive potential at anode		2.0 V	NA	81 mA	60 C	60 C
			2.2 V	NA	94 mA	60 C	60 C
			2.5 V	NA	108 mA	60 C	60 C
	Humidified O2	Liquid Water	1.5 V	0%	0 mA	60 C	60 C
	FR = 63 ml/min	FR = 10 ml/min	Positive potential at cathode				

Appendix B: MEA P1 Results

Initial Polarization Curve

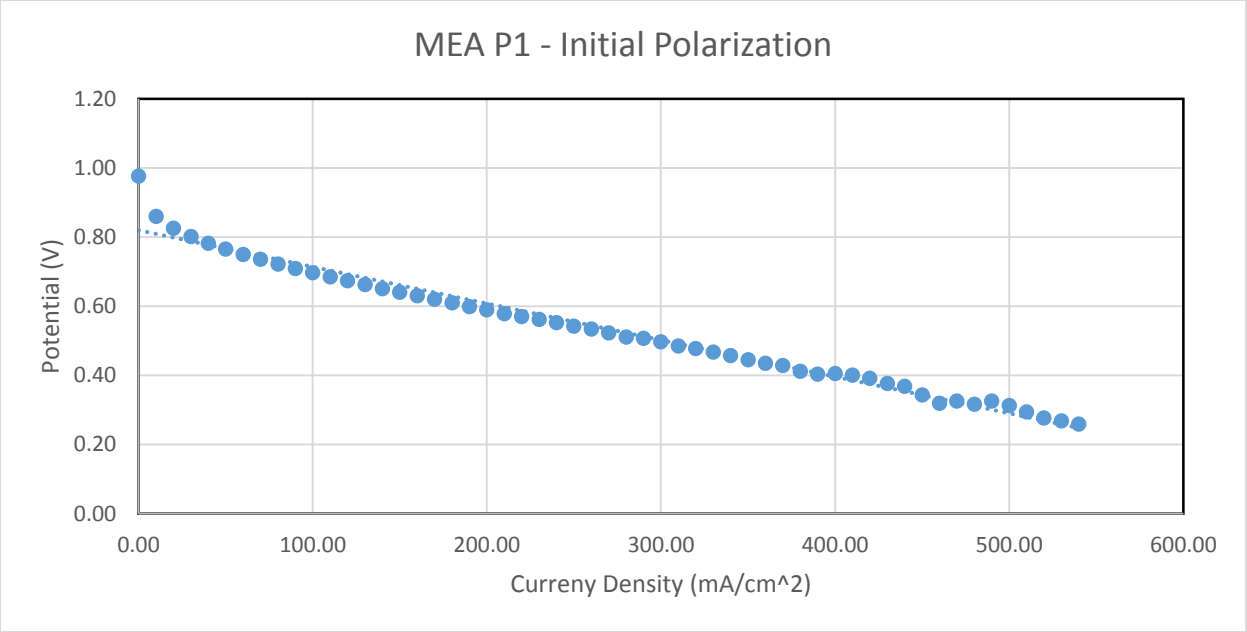

Initial Power Curve

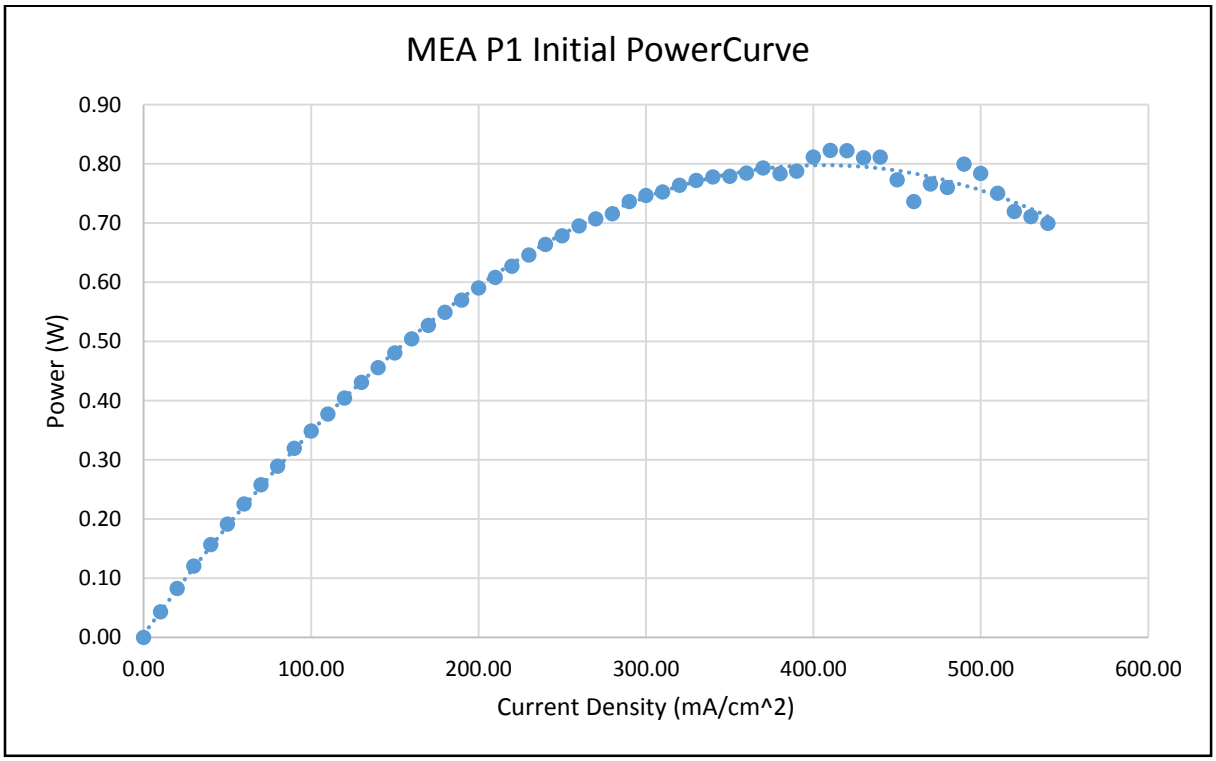

IR Spectroscopy of MEA P1

Before Experimental

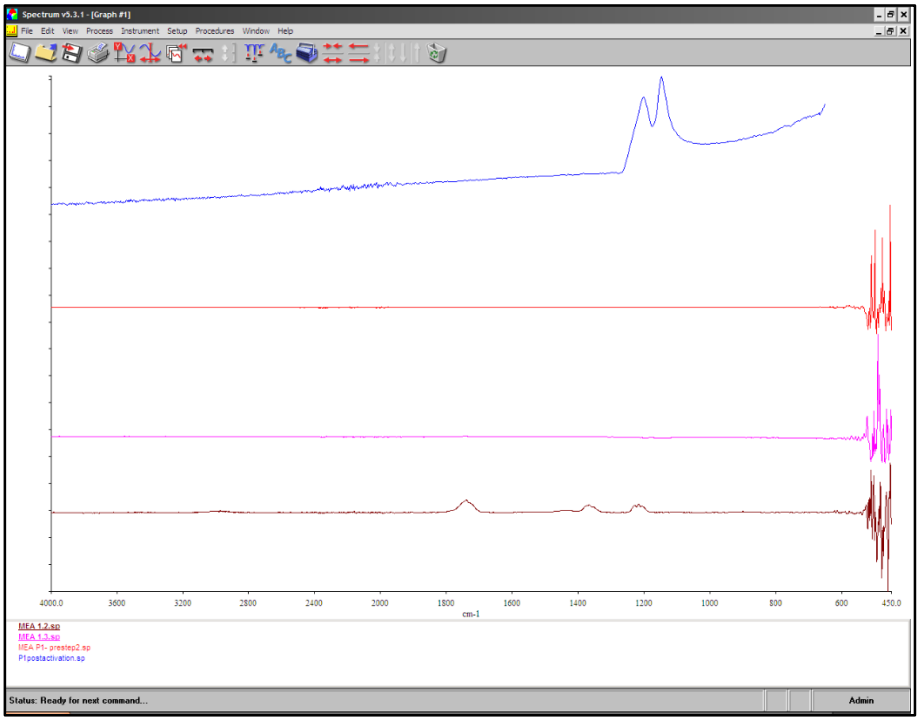

IR Specs of MEA P1. The bottom three tests are the control taken of MEA-P1 initial after opened from packaging. The top blue IR spec was taken after the condition of the membrane.

After Experimental

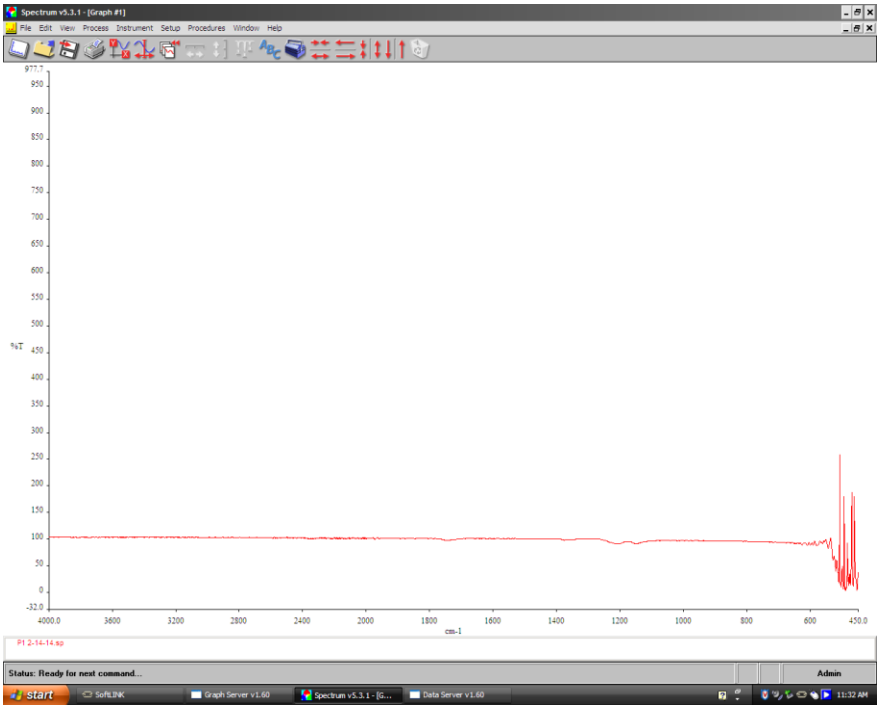

MEA P1 IR post experimental runs. It can be seen there is relatively no activity at all.

Appendix C: U.S Patent 5,211,984 for Membrane Catalyst Loading in MEA Fabrication (Wilson, 1993)

application. In another embodiment, the ionomer is provided in a thermoplastic form for high temperature pressing onto the SPE membrane.

In yet another characterization of the present invention, a SPE membrane assembly for use in a gas reaction fuel cell is formed using a Na^+ or thermoplastic form of a perfluorosulfonate ionomer to fabricate a catalyst layer. A supported Pt catalyst and a solvent are uniformly blended with the Na^+ or thermoplastic form of the ionomer to form an ink. The ink is applied to form a layer over a surface of a SPE membrane in the Na^+ form. The layer is then dried at a temperature of at least 150° C. for a Na^+ ionomer and 195° C. for a thermoplastic form of the ionomer. The resulting film and membrane are converted back to the protonated form of the ionomer to form a pliant, elastic, and coherent catalytic layer on the SPE membrane.

BRIEF DESCRIPTION OF THE DRAWINGS

The accompanying drawings, which are incorporated in and form a part of the specification, illustrate an embodiment of the present invention and, together with the description, serve to explain the principles of the invention. In the drawings:

FIG. **1** is a cross section of a fuel cell having a structure in accordance with one embodiment of the present invention.

FIG. **1A** is a pictorial illustration showing a magnified view of the catalyst layer according to the present invention.

FIG. **2** graphically depicts the performance of a thin catalyst film with 0.20 mg/cm^2 and a thicker catalyst film with 0.35 mg/cm^2 of platinum on a first SPE.

FIG. **3** graphically compares performance of thin catalyst films with 0.15 and 0.22 $mgPt/cm^2$ on a second SPE.

FIG. **4** graphically compares the performance of a thin film cathode according to the present invention with 0.15 $mgPt/cm^2$ and a commercial gas-diffusion cathode with 0.35 $mgPt/cm^2$.

FIG. **5** graphically depicts the performance of a fuel cell with a high-temperature formed, thin film catalyst layer with 0.17 gm Pt/cm^2/electrode on Membrane "C".

FIG. **6** graphically depicts the performance of a fuel cell with a high temperature formed, thin film catalyst layer with 0.13 mg Pt/cm^2/electrode on a Dow membrane.

FIG. **7** graphically compares the specific activity from a fuel cell according to the present invention and prior art fuel cells.

DETAILED DESCRIPTION OF THE INVENTION

In accordance with the present invention, a gas reaction fuel cell includes a catalyst layer adjacent the cathode surface of a solid polymer electrolyte membrane to optimize utilization of the catalyst and to minimize the amount of the included catalyst. A catalyst film may also be provided adjacent the anode surface of the solid polymer electrolyte membrane. As shown in FIGS. **1** and **1A**, catalyst layer **22** addresses three criteria necessary for a catalyst to efficiently contribute to the electrochemical processes in a fuel cell: proton access to the catalyst, gas access, and electronic continuity.

Fuel cell assembly **10** utilizes a gas fuel source **12**, gas oxidizer source **14**, solid polymer electrolyte (SPE) membrane **26** between porous anode backing structure **16** and porous cathode backing structure **18**, and at least catalyst layer **22**, according to the present invention, that is adhered to the cathode surface of SPE **26**. It will be understood that catalyst layer **30** may be disposed between membrane **26** and anode backing structure **16**. Cathode backing structure **18** is electrically connected to cathode **34** and anode backing structure **16** is electrically connected to anode **32**. The foregoing discussion applies also to catalyst layer **30**, although catalyst loadings for the anode may be significantly less than one-half the catalyst loadings required for the cathode structure. Catalyst layer **22** is formed as a film of a proton conductive ionomer **28** and a supported platinum (Pt) catalyst **24** uniformly dispersed in ionomer **28** to assure that a uniform and controlled depth of the catalyst is maintained. The resulting film is a dense film of ionomer **28** and supported catalyst **24**. i.e., there are no substantial voids in the film and there are no hydrophobic additives, such as PTFE, that block access of the diffusing gas and protons to the Pt catalyst sites. Gas access to the Pt catalyst sites is obtained through porous cathode backing structure **18** and by diffusion through ionomer **28**. A suitable ionomer, such as a perfluorosulfonate ionomer, has sufficient oxygen permeability that a diffusion pathway length of 5–10 μm does not introduce any significant oxygen transport losses through the film for an oxygen gas.

Proton penetration and gas diffusion effects of electrolyte layers, as well as the relationship between volume fraction of ionomer **28** and potential drop within catalyst layer **22**, indicate that an optimum catalyst layer **22** is very thin, i.e., a film less than 10 μm thick, and has a high volume density of supported catalyst **24** with the ionomer **28** in the interstices, i.e., the supporting carbon particles **25** are in contact with adjacent particles to form a low resistance electronic path through catalyst layer **22**. A weight ratio of about 1:3 perfluorosulfonate ionomer (dry)/Pt-C is preferred for 20 wt % supported Pt. A dense film **22** is formed that is substantially free of cavities or water pockets that lower the ionic and electronic conductivities. It will be appreciated that the thickness of film **22** is optimized when the thickness is equal to the active region for the half-cell reaction at any given current density and may be selected on the basis of the expected operating characteristics to match the catalyst thickness with a predetermined operating current density.

In one embodiment, film **22** is formed from an ink preparation including the supported catalyst, a solubilized ionomer, and one or more volatile or decomposable suspension materials to provide a viscosity suitable for film formation. The ink is spread over a release blank in one or more layers to form a film decal with a preselected concentration of catalyst. A preferred protocol is as follows:

PROTOCOL I

1. Combine a solubilized perfluorosulfonate ionomer, such as Nafion (a registered trademark of E.I. duPont Nemours) in 5% solution (from Solution Technology, Inc.) and a supported catalyst (19.8 wt % platinum on carbon from Prototech Company, Newton Highlands, Mass.) in a weight ratio of 1:3 Nafion (dry)/Pt-C. Alternate materials of perfluorosulfonate ionomer are available, such as Membrane "C" from Chlorine Engineers, Inc., of Japan and membranes from Dow Chemical Company.

2. Add water and glycerol to weight ratios of about 1:5:20 for carbon/water/glycerol.

3. Agitate the mixture with ultrasound to uniformly disperse the supported catalyst in the ink and to form the mixture to a viscosity suitable for coating the release blank.

4. Clean a release blank of teflon film and coat the blank with a thin layer of mold release (e.g., a TFE spray). Paint the blank with a layer of ink and bake in an oven at 135° C. until dry. Add layers until the desired catalyst loading is achieved.

5. Form an assembly of a polymer electrolyte membrane, counter electrode (anode electrode), and the coated blank. Place the assembly into a conventional hot press and lightly load the press until the press heats to a selected temperature (i e., 125° C. for Nafion and 145° C. for "C" SPE material) and then press at 70–90 atm for 90 seconds.

6. Cool the assembly and then peel the release blank from the film, leaving the film decal adhered to the SPE membrane cathode surface.

7. An uncatalyzed porous electrode (Prototech) is urged against the film during fuel cell assembly to form a gas diffusion backing for the thin film catalyst layer.

It should be recognized that the solubilized Nafion acts to some extent as a surfactant and dispersing agent for the supported catalyst particles. However, the dispersion of the Nafion must be controlled to provide a suitably dense film. An effective density for the present invention is obtained by simply mixing the Pt-C particles and solubilized Nafion together before the water and glycerol mixture is added.

One advantage of the dense catalyst film herein described is improved bonding of the catalyst film to the SPE membrane and continuity of the proton path. The dimensions of the SPE membrane increase considerably upon hydration of the hydrophilic material, whereas the relatively rigid carbon matrix of conventional gas-diffusion electrode structures does not significantly change dimensions upon hydration. Thus, where the catalyst is included within the carbon electrode structure, the continuity between the SPE surface and the catalyst interface can be adversely affected. The dense catalyst film according to the present invention includes a hydrophilic material as a large fraction of the catalyst film and there is less differential movement from surface expansions under hydration.

One disadvantage of forming a catalyst film decal without a binder material, such as PTFE, is that suitable ionomer materials, such as Nafion, must provide structural integrity for the film. Nafion, for example, is not melt processable and the resulting recast catalyst layer films do not have the structural integrity of commercial fluoropolymer SPE membranes. It has been found, however, that the structural integrity can be improved by heating the film to elevated temperatures for moderate amounts of time. This does cause some amount of acid-catalyzed discoloration and degradation, but the increase in structural integrity is beneficial. The film is also rendered somewhat less hydrophilic by the heating, which is beneficial at the cathode electrode where water flooding is of concern. A suitable treatment is thirty minutes exposure at 130°–135° C.

Another approach to improve the structural integrity of the catalyst layer film is to introduce a binder material that readily disperses throughout the electrode structure and imparts structural integrity at low volume fractions such that performance of the electrode is not significantly impaired. Useful catalyst layers have been prepared using polyvinyl alcohol (PVA). The surfactant nature of the PVA provides for adequate dispersion among the supported catalyst particles in an aqueous solution and the molecular structure acts to bind the carbon particles and Nafion agglomerates so that strong films are obtained with low weight fractions of PVA. Films have been formed with PVA concentrations of 10–12 wt % in the ink.

In another embodiment of the present invention, the integrity of catalyst films **22, 30** is improved and acid-catalyzed degradation of the ionomer is avoided by using the Na^+ form of the perfluorosulfonate ionomer, i.e., Nafion, to form a film for application to membrane **26** or for direct application to membrane **26**, where membrane **26** is in a Na^+ or K^+ form. The Na^+ perfluorosulfonate layer is cured at a temperature of at least 150° C., and preferably at least 160° C., and the catalyzed membrane assembly is thereafter converted to the H^+, i.e., protonated, form to complete the catalyzed membrane assembly. A preferred protocol is as follows:

PROTOCOL II

1. Prepare a mixture of Nafion and catalyst as described in Step 1 of Protocol I.

2. Add a molar amount of NaOH equal to the Nafion and mix well to convert the Nafion to the Na^+ form.

3. Form an ink as in Steps 2 and 3 of Protocol I.

4. Provide a membrane of Na^+ Nafion by soaking a protonated membrane in a solution of NaOH, followed by rinsing and drying, or by procuring the membrane in a Na^+ or K^+ form.

5. Apply the ink directly to one side of the membrane. The amount of catalyst applied to the membrane is determined from the amount of ink transferred to the surface. Typically, two coats are required to obtain the desired catalyst loading. In one method of drying the ink, the ink-coated membrane is placed on a vacuum table having a fine sintered stainless steel filter on top of a heated vacuum manifold plate. A silicone blanket having a cut-out area the size of the membrane area to be inked is placed over the membrane to seal the uncovered areas of the vacuum table about the membrane. The vacuum table is operated at a temperature of at least 150° C., and preferably about 160° C., as the ink is applied. The vacuum appears to prevent distortion of the membrane from solvents in the ink and to yield a smooth, uniform film. The high-temperature application and drying appears to cure the catalyst layer to a film of high integrity and that is pliant and elastic. The second side of the membrane may be coated in the same manner.

6. Optionally, the assembly is hot pressed at 70–90 atm at 185° C. for about 90 seconds.

7. The assembly is converted back to the protonated form by lightly boiling it in 0.1M H_2SO_4 and rinsing in deionized water. The assembly is air dried and combined with an uncatalyzed porous electrode as in Step 7 of Protocol I.

Alternately, the Na^+ form of ink (Steps 1–3, above) and membrane may be used in Protocol I to form a separate catalyst film for application to the membrane.

The high-temperature casting of Na^+ Nafion films to improve film integrity is generally suggested in Moore et al., "Procedure for Preparing Solution-Cast Perfluorosulfonate Ionomer Films and Membranes," 58 Anal. Chem., pp. 2569–2570 (1986), incorporated herein by reference. The article suggests that solvents such as

dimethyl sulfoxide (DMSO) might yield equivalent properties to glycerol solvents, described above, but at lower process temperatures. The above protocol appears to yield equivalent cell performance with both DMSO and glycerol solvents. DMSO does provide a good suspension medium for the solids, however, and may form a good solution for a spray application of ink to the membrane surface.

In yet another embodiment of the present invention, the robustness, i.e., integrity, of the film decal is improved by using a thermoplastic form of a perfluorosulfonate ionomer in the ink solution. The thermoplastic form is obtained by ion-exchange of a hydrophobic cation, such as tetra-butyl ammonium hydroxide (TBAOH) with the proton form of the ionomer. Suitable hydroplastic cations are relatively large molecules (compared to normal cations, e.g., Na^+) with hydrophobic organic ligands, such as tetra-butyl ammonium, tetra-propyl ammonium, and the like.

The resulting thermoplastic film on the SPE membrane can now be hot pressed against the membrane at a temperature above the deformation temperature of the perfluorosulfonate ionomer in order to effectively adhere to the SPE membrane. The SPE membrane material is supplied in a Na^+ form and the resulting assembly is converted to the protonated form for use in the fuel cell assembly. A preferred protocol is as follows:

PROTOCOL III

1. Prepare a mixture of perfluorosulfonate ionomer, such as Nafion or membrane "C" material, and catalyst as described in Step 1 of Protocol I.

2. Add a molar amount of TBAOH equal to the ionomer to convert the ionomer to the thermoplastic TBA^+ form.

3. Form an ink as in Steps 2 and 3 of Protocol I.

4. Provide a membrane of Na^+ perfluorosulfonate ionomer as in Step 4 of Protocol II.

5. Apply the ink to the membrane either by decal preparation (Steps 4–6 of Protocol I) or directly to the membrane (Step 5 of Protocol II).

6. Hot press the catalyst layer of the membrane assembly at a temperature above the deformation temperature of the converted ionomer, i.e., preferably at about 195° C., at 70–90 atmospheres for a time effective to form a glassy, smooth finish, e.g., about 90 seconds.

7. Convert the assembly back to a protonated form (Step 7, Protocol II).

The thermoplastic form of the ink is readily applied as either a decal or an ink. Both forms adhere well to the SPE membrane and the hot press at the higher temperature enables the thermoplastic material to deform onto the membrane for an adherent and continuous interface.

FIGS. 2–7 graphically depict the performance of fuel cells prepared according to the present invention. All of the ink formulations were prepared using supported catalysts of 19.8 wt % platinum on XC-72 carbon powder (Prototech) mixed with Nafion. The cathode electrodes for mating with the catalyst layer were conventional PTFE bonded electrodes with no catalyst (Prototech). The fuel cells whose performance is shown in FIGS. 1-4 have cathodes prepared according to Protocol I and include conventional anodes (Prototech) with a catalyst loading of 0.35 mg Pt/cm^2 plus a sputter coat of 500 Å Pt. It will be understood that conventional anode electrodes were used to provide performance comparisons of cathode electrodes.

The anode catalyst loading is not expected to have any significant effect on cell performance, Indeed, the fuel cells whose performance is shown in FIGS. 5 and 6 include high temperature catalytic layers on both the cathode and anode faces of the membrane. Both catalytic layers incorporated equivalent catalyst loadings, e.g., 0.13 mg Pt/cm^2, for a total cell loading of 0.26 mg Pt/cm^2 of electrode surface. Anodes with catalyst loadings as low as 0.03 mg Pt/cm^2 have shown little degradation in fuel cell performance.

FIG. 2 graphically depicts the voltage vs. current density curves for fuel cells having conventional Prototech anodes, Nafion 117 (7 mil thick) SPE membrane, and a cathode assembly with a catalyst layer produced by mixing Pt/C catalyst and Nafion and hot pressed onto the SPE membrane Catalyst loadings of 0.20 and 0.35 mg Pt/cm^2 are compared using both neat oxygen and air as the oxidant. It is readily seen that the thinner catalyst layer (0.20 mg Pt/cm^2) performs somewhat better than the thicker film (0.35 mg Pt/cm^2) at higher current densities. At the higher current densities, the active region of the catalyst layer narrows and less of the film thickness is utilized, wherein mass transfer losses increase in the thicker film and performance decreases. The low partial pressure of oxygen in air as compared to neat oxygen induces an earlier and steeper fall-off in performance at the higher current densities.

FIG. 3 graphically depicts the voltage vs. current density curves for fuel cells constructed as the fuel cells of FIG. 2, except that the SPE membrane is Membrane "C" (a perfluorosulfonate membrane from Chlorine Engineers Inc. of Japan). Catalyst loadings of 0.15 and 0.22 mg Pt/cm^2 are compared, again using both neat oxygen and air as oxidizers. The results are consistent with the results shown with Nafion 117 forming the SPE membrane, with lower potentials from the thicker film at higher current densities.

The performance of the fuel cells depicted in both FIGS. 2 and 3 approach those of fuel cells fabricated with conventional Prototech cathode assemblies or of assemblies using unsupported Pt catalyst with much higher Pt loadings FIG. 4 particularly compares the cell voltage vs. current density performance of a thin catalyst layer with a loading of 0.15 mg Pt/cm^2 with a cell having the catalyst included in a carbon electrode to a loading of 0.35 mg Pt/cm^2 with an extra sputter coating of 500 Å Pt. The substantial similarity in performance is readily apparent.

The performance of fuel cells formed by a direct application of a Na^+ ink to a Na^+ membrane is shown in FIGS. 5 and 6. FIG. 5 depicts the performance of the high-temperature, thin film formed on Membrane "C" according to Protocol II, wherein the cell performance on oxygen is at least equal to the performance of the separate thin film cell shown in FIG. 4. FIG. 6 depicts the performance of the high-temperature, thin film formed on a "Dow" membrane according to Protocol II, wherein an improved cell performance is obtained. The "Dow" membrane is a proton conducting membrane available from the Dow Chemical Company. It is quite significant that a low Pt loading of 0.13 mg Pt/cm^2 is effective to generate current densities of above 3 A/cm^2 at a cell voltage higher than 0.4 V for operation on pressurized oxygen and, particularly, that such a low loading is effective to reach a cell voltage of 0.65 V at 1 A/cm^2 for cells operated on pressurized air.

To further illustrate the significant increase in catalyst utilization efficiency afforded by the present inven-

tion, FIG. 7 depicts cell voltage as a function of the specific activities of the cathodes (A/mgPt) for fuel cells with four different cathode catalyst configurations: (1) a thin film catalyst loading of 0.15 mg Pt/cm^2, as taught herein; (2) a high-temperature thin film with a catalyst loading of 0.13 mg Pt/cm^2 applied directly to the membrane as an ink; (3) a commercial Prototech electrode with a catalyst loading of 0.35 mg Pt/cm^2 and 500 Å Pt coating; and (4) GE/HS-UTC-type cell with 4 mg Pt/cm^2 (unsupported) hot pressed into the SPE. It should be noted that the GE/HS-UTC-type cell has hardware, membrane design, and operating conditions that are significantly different from the other cells and its performance comparison is merely illustrative. The differences in the specific activities for each type of electrode are clearly significant, with the thin film supported catalyst layers according to the present invention being the most efficient utilization of the Pt catalyst.

Fuel cell performance using catalyzed membranes formed with the TBA+ form of the perfluorosulfonate ionomer is generally the same as the performance obtained from membranes formed with the Na+ form of the ionomer as shown in FIGS. 5-7.

Thus, it will be appreciated that the present invention obtains a high catalyst utilization by the improved construction of the catalyst layer with low Pt loadings primarily involving increased contact area between the polymer electrolyte and the Pt catalyst clusters. The contact area is increased in two ways. First, the supported catalyst and the ionomeric additive are cast together to form the catalytic layer, wherein the catalyst has a very high weight fraction of ionomer (about 25 wt %) compared with the weight fraction from the impregnated electrode structure of the '115 patent (about 10 wt %). Second, the hydrophobic additive is completely eliminated and the ionomer is uniformly dispersed throughout the catalyst layer. The latter is accomplished by blending the solubilized ionomer and the platinized carbon into a homogeneous "ink," from which the thin film catalyst layer is formed.

FIGS. 2 and 3 illustrate the significance of film thickness affecting proton penetration and gas access and the resulting cell performance. As current density increases, the active catalyst region narrows. Thus, the oxidizer gas and/or protons must diffuse through inactive portions of the catalyst layer and, in the case of air, the mass transfer limitation further increases the overpotential. An electrode thickness roughly equivalent to that of the active region at a particular current density would provide an optimum performance at that current density. For example, with 20 wt % Pt/C supported catalyst and a catalyst layer fabricated in accordance with the above principles, reasonable fuel cell performance is obtained down to about 0.1 mg Pt/cm^2, after which it falls off in proportion to further decrease in catalyst loading. Concomitant film thicknesses are in the range of 1-10 μm, and preferably 2 to 3 μm. It is observed that catalyst loadings as low as 0.03 mg Pt/cm^2 may be used for an anode catalyst layer without significant loss of performance. Improved performance might be obtained from a given catalyst layer thickness if a higher Pt loading could be included without increasing the thickness of the supported catalyst.

The foregoing description of the preferred embodiments of the invention have been presented for purposes of illustration and description. It is not intended to be exhaustive or to limit the invention to the precise form disclosed, and obviously many modifications and variations are possible in light of the above teaching. The embodiments were chosen and described in order to best explain the principles of the invention and its practical application to thereby enable others skilled in the art to best utilize the invention in various embodiments and with various modifications as are suited to the particular use contemplated. It is intended that the scope of the invention be defined by the claims appended hereto.

What is claimed is:

1. A method for fabricating a SPE membrane assembly for use in a gas reaction fuel cell, comprising the steps of:
   - furnishing a SPE membrane in Na+ form;
   - furnishing a perfluorosulfonate ionomer in a Na+ form or thermoplastic form;
   - uniformly dispersing a supported Pt catalyst and a solvent in said Na+ or said thermoplastic form of said ionomer to form an ink;
   - forming a film of said ink containing a predetermined amount of said catalyst on a surface of said SPE membrane in said Na+ form;
   - heating said film of said ink to a temperature effective to dry said ink; and
   - converting said film of said ink and said SPE membrane to a protonated form of perfluorosulfonate.

2. A method according to claim 1, wherein the step of furnishing said perfluorosulfonate ionomer in a Na+ form includes the step of adding NaOH to a protonated form of said perfluorosulfonate ionomer.

3. A method according to claim 1, further including the step of maintaining said membrane in a planar condition on a vacuum table while forming said film of said ink on said membrane.

4. A method according to claim 1, wherein the step of furnishing said perfluorosulfonate ionomer in a thermoplastic form includes the step of ion-exchange of a hydrophobic cation with said perfluorosulfonate.

5. A method according to claim 4, wherein said hydrophobic cation is tetra-butyl ammonium.

* * * * *

Appendix D: Sample plot generated by COMSOL.

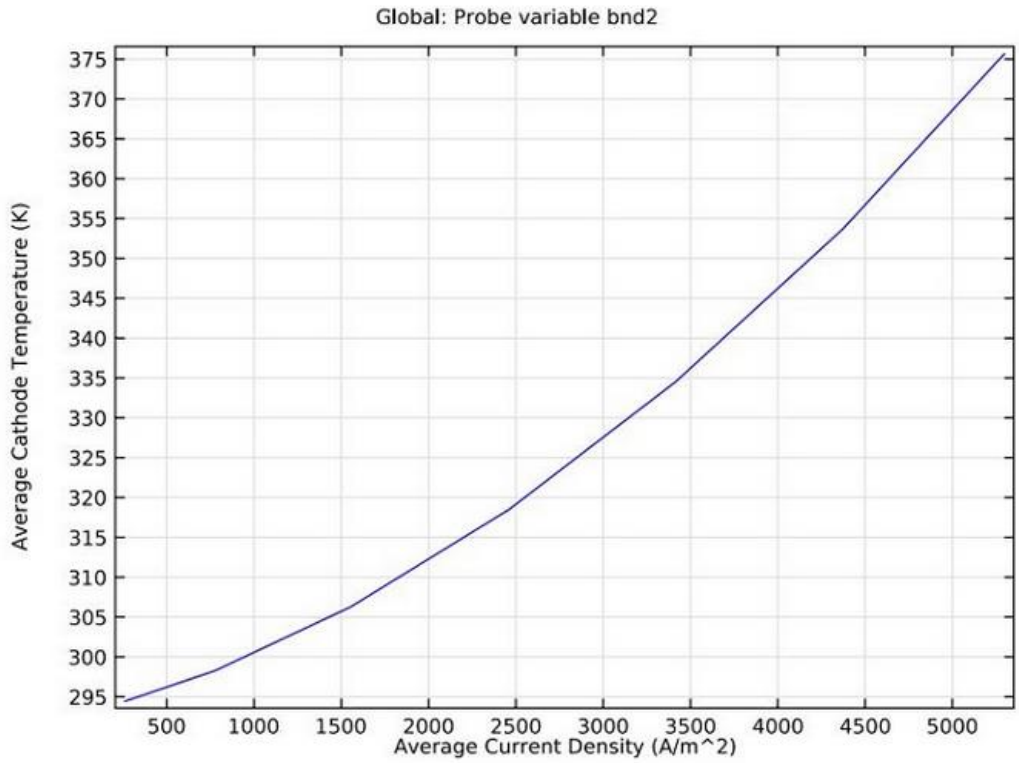

Cathode average temperature dependence on average current density.